Bond graph modeling of a typical flapping wing micro-air-vehicle with the elastic articulated wings

Saeed Karimian · Zahra Jahanbin

Abstract In the present research, a new comprehensive model of a flexible articulated flapping wing robot using the bond graph approach is presented. The flapping kinematics of a two-section wing is introduced via the bond graph based approach on a hybrid mechanism providing amplitude and phase characteristics. The aerodynamic quasi-steady approach equipped with stall correlation is utilized according to the reduced flapping frequency and the angle of attack ranges. The local flow velocity and the wing position are calculated in both wing and body coordinates taking into account rotation and translation of the wing different parts. Estimation of the effective angle of attack is performed by calculating the instantaneous torque distribution on both wing sections. Aeroelastic modeling is employed in which the wing structure is assumed as an elastic Euler–Bernoulli beam at the leading edge with three linear torsional modes. In this novel integrated bond graph model, computation of the performance indices including the average lift and thrust, consumed and produced powers by flapping and mechanical efficiency are presented. Due to existence of the numerous geometric and kinematic parameters in articulated flexible flapping wing, such a model is essential for design and optimization. Consequently, an example of a typical parametric study and the results validation are carried out. It is indicated that the sensitivity of the bird performance to relative change in design variables would increase for out of phase flapping, second part stiffness, flapping amplitude, frequency and velocity respectively. It is interesting that by employing the reverse-phase flapping which is possible only via articulated wings, the maximum efficiency could be achieved. In addition, it is shown that adjusting the wing torsional stiffness is a crucial item in design of passive flapping robots. The key advantage of the two-section flapping wing is depicted as the controlling capability of the angle of attack in the outer part of the wing. Finally, the improved version of the bird is being addressed by approximately 15% progress in propulsive efficiency.

Keywords Elastic articulated wings · Flapping wing · Bond graph approach · Aerodynamic model · Flight dynamic characteristics

S. Karimian (✉) · Z. Jahanbin
Aerospace Group, Faculty of Mechanical Engineering, Tarbiat Modares University, Tehran, Iran
e-mail: Karimian@modares.ac.ir

Z. Jahanbin
e-mail: zahrajahanbin@modares.ac.ir

1 Introduction

The humankind has always been enchanted by the magic of the bird's flight, and always admires its beauty and complexity. The perfect harmony between the bird physical structure and the functions of their

body organs, and understanding the relationship between the physiology of birds with the scientific principles and rules is very interesting [1]. The bird is an efficient and superior flying vehicle with more than 150 million years of evolution. Men have always dreamed to fly while watching the flying birds. The birds are capable of flying efficiently in their flight maneuvers, take off and landing with the ease of appearance through their two-section wings in contrast to the approach used to fly the relatively simple human-made planes with the fixed and rotary wings. The complex aerodynamic based on the flapping flight is a usual challenge in investigating the birds flight, and scientists are hopeful to discover and reveal the secrets of the bird's flight [2]. Nowadays, the researches on the flapping aircrafts have increased significantly due to the weight loss of equipment mounted on them, including their sensors and actuators. However, there is a lack of studies on the articulated flapping wings, and it would be very difficult to find the commercial articulated wing birds [3]. It is logical to inspire from the nature in the efforts to design a small-scale aerial vehicle. Constructing the wings that are more similar to the biological two-section wings and analyzing their performance, one can get a better insight of implementing these wings in a flapping bird, and become closer to imitating the flight of the birds [2].

The flapping birds with two-section wings have more aerodynamic and bionic advantages than the single-section wings. The two-section flapping wings have flapping, twisting and folding movements that make their flying performance much closer to the real birds [4]. Some of the most important advantages of the articulated flapping wings are their greater similarity to the large-scale wings of the real birds, the possibility of the aerodynamic improvement of the wing tip, the probability of the greater control over the aerodynamic and dynamic parameters of the bird, the capability of the lateral control with more degrees of freedom, and the opportunity of using the modern actuators such as smart alloys, shape memory alloys, piezo actuators and macro fiber composites. Of course, the use of the articulated wings in modeling process have some disadvantages, such as increasing the weight of their connections and links, as well as the complexity of designing such birds, but these disadvantages can be neglected comparing to their advantages. However, there are very few studies focusing on

the articulated wings with folding capability and the researches in this field are not sufficient [5]. The simulated movements of the wings still are not able to imitate all of the birds' flying characteristics, and their flight flexibility and aerodynamic efficiency are limited [4].

Among the studies on the articulated flapping wings, the Kim et al. [3] research on design, fabrication, and flight test of the articulated ornithopter can be mentioned. In this study, a two-section flapping bird with the flapping frequency of 2–3 Hz has been simulated based on the kinematic analysis, and the results have been validated using MATLAB, Solid-Works and ADAMS computer softwares. Finally, design parameters have been analyzed using the motion capture cameras. In another study, Hua et al. [4], numerically analyzed the aerodynamics of a three-section flapping wing based on the realistic flying features of the real birds through the numerical simulations. For this purpose, a flapping mechanism was designed for a three-section flapping wing to simulate both flapping and double folding motions, and to study the aerodynamic characteristics of the great birds. In addition, the aerodynamic performance of a three-section flapping wing under the typical flight conditions was compared to the two-section wing, and it was proved that the three-section flapping wing has better aerodynamic performance than the two-section wings. Chand et al. [6] focused on design analysis, modelling and empirically validation of a relatively new generation of the full-scale two-section flapping wing robots. In this study, the Euler angles have been used rather than the Quaternions in the dynamical model to show the flight direction of the flying ornithopter in the three-dimensional space for providing smoother rotational maneuvers using the spherical linear interpolation. The main objective of this paper was on the autonomous control of the bird. Stowers and Lentink [7] presented the results of the flapping wing passive morphing based on the experimental outcomes of the predictive dynamical model, and the dimensional analysis of a passively unfold wing. The purpose of their research was to illustrate the ability of the two-section wings to unfold without any additional actuation while the wings flap. Moreover, for better understanding the bird passive dynamics, a computer model of the wing unfolding process was constructed based on the rigid body dynamics in the Motion Genesis software, which linked the model and the

aerodynamic relationships to each other. Srigrarom and Chan [8] developed a sample flapping bird that mimics the flapping movement of the birds' articulated wings, and examined the lift and propulsive forces characteristics for various wing designs. This research focused on the arrangement of the wing main spar as well as the materials used for constructing the wings, which can improve the wings performance. In addition, in order to understand the mechanism for producing the required lift, different techniques for measuring lift and thrust forces were used. Shams et al. [9] conducted an investigation to calculate the aerodynamic forces of a two-section flapping bird with seagull characteristics. This flapping bird which produces lift and thrust forces with the help of the up and down stroke movements of its two-section wings was simulated assuming the quasi-steady aerodynamic, the wings phase lag, and the rigid four bar mechanism for each of the wings sections. Guerrero et al. [10] presented the initial design of an unmanned aerial vehicle with two-section wings, inspired by biology. The numerical studies were performed on the proposed bird model to evaluate the aerodynamic performance and the flight stability in both gliding and flapping states. Moreover, shape, size, and flight conditions of the model were considered for estimating the performance of a seagull. Negrello et al. [11] presented the initial kinematic and geometric design of a flapping bird, which has the ability to carry out the video surveillance and the reconnaissance missions under the mechanical constraints by the use of the fluid dynamics. In order to define the dimensional characteristics of the flapping vehicle, at first the biological study has been done, such as the weight-to-span ratio analysis for proper flight kinematics. On the other hand, the different flapping mechanisms were analyzed in order to find the best way to produce the flapping motion of the articulated wings. In addition, the flight stability and the flapping effects on the flight dynamics were investigated. In addition to these researches, the highly acclaimed results of an artificial hinged-wing bird model have been introduced by a German research group under the supervision of the Festo commercial company [12]. The introduced smart bird has been studied using two new flying features inspired by the biological nature of the birds, namely the active wing torsion and the partial linear kinematics.

Since the under investigation flapping robot system has been composed of a combination of the mechanical, electromagnetic, and the aerodynamic systems, the exclusive bond graph method which is the great tool for modeling the multiphase systems and calculating the energy efficiency, can be utilized for modeling the flapping ornithopters. The bond graph method is applicable to a wide range of the complex dynamic and the multidisciplinary systems, specially the mechanical and the electrical systems, as well as the chemical, fluid, thermodynamic, ecological, magnetic, and biomedical and many other systems [13]. In the last decades, using this method as a common approach have significantly become into consideration in many design and engineering fields, including the simulation of the electrical [14, 15] and the power transmission [16, 17] systems, as well as the multibody mechanical [18–20] and the mechatronic [21–24] mechanisms. In the field of the complete modeling of the unmanned aerial vehicles in micro and nano scales, especially the intended flapping type, limited researches have been conducted using the bond graph method. Bontemps et al. [17] focused on the power modeling of a flapping wing nano-air-vehicle power transmission system and its electromagnetic engine in order to investigate the transmitted power to the wings from the power source; hence, the improvement of the actuation efficiency would be possible. The main objective was to develop the power system of an insect like flapping robot in terms of the kinematics and the scale using the MEMS technologies. Due to the prototype multiphysics nature, the Bond Graph formalism have been used as a tool for modeling such a multiphysics system and its energetic analysis. In addition, the results have been validated with the experimental results, and the model efficiency has been determined. However, the whole configuration of the flapping bird was not presented. Dupont et al. [25] developed the bond graph modelling in the field of the flapping wing micro-air-vehicle aerodynamics for investigating the flapping flight performance in nature. The dynamic model of a flapping bird with a main body and two wings was presented using the Newton–Euler formulation with a fixed body coordinate system. Some simplifications and assumptions, such as considering wings as rigid beams, neglecting wings mass and inertia and considering the body aerodynamic forces. Although in this research, a complete description of the system, including the

power transmission, the dynamic behavior of the system and the wing modeling has been carried out, there is a need to improve and overcome the modeling defects, such as the wings bond graph model. Doan et al. [26] presented a numerical model based on the bond graph approach for a simple micro flapping robot, in order to analyze and investigate wing kinematics and overall estimation of the lift force. In this bond graph model, the quasi-steady aerodynamic theory and the Lagrange dynamic equation were considered as the basic principles. In addition, wing kinematics which enhances the total lift force has been derived based on the non-linear optimization of the system sensitivity parameters including the spring stiffness, the working frequency, the input voltage and etc. However, in this study the bond graph modeling of the body and the flapping mechanism has been neglected. Jahanbin et al. [27] examined the possibility of modeling a flapping wing robot utilizing the bond graph method, and indicated that the proposed model not only eliminates the complexity of modeling such complicated systems, but also provides useful information about the power flow between the bird different subsystems. Since the purpose of this study was to simulate the wings flapping motion in a hovering flight, various simplifications, such as considering one-section rigid wings as the rigid Euler–Bernoulli beam, as well as neglecting the aerodynamic forces, were made. In another study, Jahanbin and Karimian [28] followed their former research, and tried to do the parametric study of an elastic flapping robot in a hovering flight neglecting the aerodynamic forces. In this regard, the effects of various mechanical and electrical parameters such as wings flexibility, relocation of the forced point of action, motor initial inertia, torsional spring stiffness and wings phase lag, on the elastic deflection of the wings, the concentrated applied force to the wing and the flapping angle, were investigated. It was shown that the bond graph method could simplify the parametric study of such complex systems. Furthermore, an integrated and systematic modeling of all components and subsystems of a single-section flapping wing was developed using the bond graph method by Karimian and Jahanbin [29]. The wings kinematics was independently implemented with the aim of evaluating the flapping bird lateral movements, and the aerodynamic forces were

extracted assuming the quasi-steady theory. Moreover, the performance evaluation of the flapping bird was carried out with the parametric study around the important quantities, such as frequency, velocity, torsional stiffness and flapping amplitude, which resulted in attractive and applicable consequences. In addition, the ability of the flapping wing robot to create the lateral forces without using any additional control surfaces and only by creating the asymmetry in the pattern of wing flapping was studied in order to perform the transverse or lateral maneuvers. Finally, it was shown that based on the proposed bond graph model, it would be possible to study the effect of design variables, mechanical characteristics, geometrical constraints, and especially bird kinematics on a wide range of the performance parameters.

Regarding the bond graph modeling of the articulated flapping wings, there is no meticulous and comprehensive work. Therefore, in this paper, it would be tried to provide an inclusive and systematic bond graph model of the articulated flapping wing various components. This modeling process provides the basic framework for many other research activities in the field of performance and stability analysis, controller design, kinematic and structural optimization, and the evaluation of the similar flapping birds. Subsequently, to achieve such modeling in bond graph environment, first the subsystems models are presented including the mechanism, wing, body and the tail of the bird, then these subsystems are interconnected and linked together as a unified set. In particular, and as a major achievement of this activity, two-section wing modeling with a middle hinge-point constraint, considering all degrees of freedom is elaborated in detail. The kinematics of the wing both sections are provided by a new hybrid mechanism, which is composed of 4-bar and 5-bar mechanisms, respectively for first and second sections of the wings. In this modeling, not only the quasi-steady aerodynamics with force coefficients correction is utilized, but also for estimating the twisting angles of the wing sections, the coupling behavior of the aeroelastic interaction is also considered. The impact of any design variables or control parameters on the bird performance can be easily studied through this integrated and systematic model.

2 The governing equations of the flapping wing subsystems

The under investigation flapping ornithopter in this study includes the main body, the two-section wings with the span of 1 m, a pair of DC motors and power transmission systems. In this section, the governing equations of the main components of the power system (propulsion and power transmission systems), two-section wings and the main body, which are modeled with the help of the bond graph method, are presented.

2.1 Power system

Figure 1 illustrates the schematic diagram of the presented bird power system, including the propulsion system and the power transmission mechanism. In this system, a pair of DC motors is used as the propulsion system. The motor armature consists of an inductance and a resistance that converts the electrical energy to the mechanical one. The motor characteristics include the armature voltage E_a, the nominal voltage V_t, the armature current I_a, the armature resistance r_a and the armature inductance L_a. The governing differential equations of this model are as follows:

$$\begin{cases} \dfrac{d}{dt}I_a = -\dfrac{r_a}{L_a}I_a - \dfrac{K_v}{L_a}\omega_a + \dfrac{V_t}{L_a} \\ \dfrac{d}{dt}\omega_a = \dfrac{K_t}{J}I_a - \dfrac{B}{J}\omega_a - \dfrac{T_L}{J} \end{cases} \quad (1)$$

In the above equations, ω_a, K_v, J, B, K_t and T_L, respectively are the angular velocity, the armature

velocity constant, the motor moment of inertia, the friction constant, the motor torque constant and the friction torque of the motor. In the proposed flapping bird, for each of the wings, a combination of 4-bar and 5-bar mechanisms is utilized as a power transmission system to independently create the flapping motion of each section of the wing, according to Fig. 1. The mechanisms are designed in such a way that the two links are attached to the crank (main gear) at two different radiuses of the crank and with a certain phase difference.

The attached link to the crank at a smaller radius is connected to the first section of the wing, the attached link to the crank circumference is connected to the second section of the wing, and they produce the flapping motion of both wing sections with the crank rotation (Fig. 1). The source of flow supplied by the DC motor is considered as the input of the mechanisms. The kinematic equations of the flapping mechanism are extracted as follows. In order to extract the linear and angular velocities of the center of mass of link d_1 connected to the first section of the wing, we have:

$$\vec{V}_{A_1} = \frac{d}{dt}\begin{bmatrix} r_1 \cos \lambda_1 \\ r_1 \sin \lambda_1 \end{bmatrix} = \begin{bmatrix} -r_1 \dot{\lambda}_1 \sin \lambda_1 \\ r_1 \dot{\lambda}_1 \cos \lambda_1 \end{bmatrix} \quad (2)$$

$$\vec{V}_{B_1} = \frac{d}{dt}\begin{bmatrix} -e + l_1 \cos \gamma_1 \\ h + l_1 \sin \gamma_1 \end{bmatrix} = \begin{bmatrix} -l_1 \dot{\gamma}_1 \sin \gamma_1 \\ l_1 \dot{\gamma}_1 \cos \gamma_1 \end{bmatrix} \quad (3)$$

In the above relations, $\vec{V}_{A_1}$ and $\vec{V}_{B_1}$ are respectively the linear velocity vectors of the points A_1 and B_1 (the

Fig. 1 The schematic diagram of the power system of the presented flapping wing
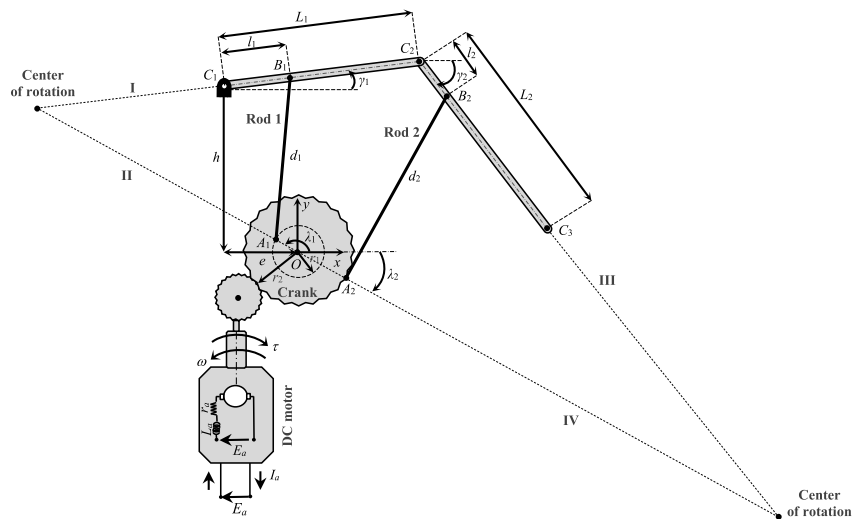
beginning and end-points of link d_1), r_1 is the radius of the crank in which the d_1 link is attached and l_1 is the connection point of link d_1 to the first section of the wing. Moreover, e and h represent the horizontal and vertical distance between the hinge points of the wing to the body, γ_1 is the flapping angle of the wing first section, and λ_1 is the instantaneous angle of the connection point of d_1 link (point A_1). Now, knowing the linear velocities of the beginning and the end pointsof d_1 link, the linear velocity of mass center of this link can be calculated as follows:

$$\vec{V}_{x_{d_1}} = -\left(\frac{1}{2}r_1 \sin \lambda_1\right)\dot{\lambda}_1 - \left(\frac{1}{2}l_1 \sin \gamma_1\right)\dot{\gamma}_1 \qquad (4)$$

$$\vec{V}_{y_{d_1}} = \left(\frac{1}{2}r_1 \cos \lambda_1\right)\dot{\lambda}_1 + \left(\frac{1}{2}l_1 \cos \gamma_1\right)\dot{\gamma}_1 \qquad (5)$$

In order to calculate the angular velocity of link d_1, according to the geometry of the mechanism and finding the instantaneous center of rotation, which is obtained by intersecting directions perpendicular to $\vec{V}_{A_1}$ and $\vec{V}_{B_1}$. The equations of line I and II are respectively derived as follows:

$$y - h = (x + e)\tan \gamma_1 \qquad (6)$$

$$y = x \tan \lambda_1 \qquad (7)$$

From the intersection of lines I and II, the coordinate of the instantaneous center of rotation point is obtained as follows:

$$x_{cr} = \frac{e \tan \gamma_1 + h}{\tan \lambda_1 - \tan \gamma_1} \qquad (8)$$

$$y_{cr} = \tan \lambda_1 \frac{e \tan \gamma_1 + h}{\tan \lambda_1 - \tan \gamma_1} \qquad (9)$$

$$r_{cr} = \sqrt{x_{cr}^2 + y_{cr}^2} - r_1 \qquad (10)$$

In which, r_{cr} is the distance between the instantaneous center of rotation and point A_1. x_{cr} and y_{cr} are the instantaneous center of rotation point coordinates. Therefore, the angular velocity of link d_1 is obtained as:

$$\omega_{d_1} = \left(\frac{1}{\sqrt{x_{cr}^2 + y_{cr}^2} - r_1}\right)r_1\dot{\lambda}_1 \qquad (11)$$

In addition, in order to extract the linear and angular velocities of the center of mass of link d_2 attached to

the second section of the wing, the following equations are used:

$$\vec{V}_{A_2} = \frac{d}{dt}\begin{bmatrix} r_2 \cos \lambda_2 \\ r_2 \sin \lambda_2 \end{bmatrix} = \begin{bmatrix} -r_2\dot{\lambda}_2 \sin \lambda_2 \\ r_2\dot{\lambda}_2 \cos \lambda_2 \end{bmatrix} \qquad (12)$$

$$\vec{V}_{B_2} = \frac{d}{dt}\begin{bmatrix} -e + L_1 \cos \gamma_1 + l_2 \cos \gamma_2 \\ h + L_1 \sin \gamma_1 + l_2 \sin \gamma_2 \end{bmatrix}$$
$$= \begin{bmatrix} -L_1\dot{\gamma}_1 \sin \gamma_1 - l_2\dot{\gamma}_2 \sin \gamma_2 \\ L_1\dot{\gamma}_1 \cos \gamma_1 + l_2\dot{\gamma}_2 \cos \gamma_2 \end{bmatrix} \qquad (13)$$

In the above equations, $\vec{V}_{A_2}$ and $\vec{V}_{B_2}$ are the linear velocity vectors of points A_2 and B_2 (the beginning and end-points of link d_2). r_2 is the crank radius and l_2 is the connection point of link d_2 to the second section of the wing. γ_2 is the flapping angle of the wing second section and λ_2 is the instantaneous angle of the connection point of link d_2 (point A_2). Now, having the linear velocities of the begginig and end-points of link d_2, the linear velocity of the link center of mass can be calculated as follows:

$$\vec{V}_{x_{d_2}} = -\left(\frac{1}{2}r_2 \sin \lambda_2\right)\dot{\lambda}_2 - \left(\frac{1}{2}L_1 \sin \gamma_1\right)\dot{\gamma}_1$$
$$- \left(\frac{1}{2}l_2 \sin \gamma_2\right)\dot{\gamma}_2 \qquad (14)$$

$$\vec{V}_{y_{d2}} = \left(\frac{1}{2}r_2 \cos \lambda_2\right)\dot{\lambda}_2 + \left(\frac{1}{2}L_1 \cos \gamma_1\right)\dot{\gamma}_1$$
$$+ \left(\frac{1}{2}l_2 \cos \gamma_2\right)\dot{\gamma}_2 \qquad (15)$$

Now, the superposition principle is used for calculating the angular velocity of link d_2, and it is assumed that ω_{d_2} is resulted from the two different movements, which are combined together as follows:

$$\omega_{d_2} = \omega_{d_2}^{\dot{\gamma}_1} + \omega_{d_2}^{\dot{\gamma}_2} \qquad (16)$$

where $\omega_{d_2}^{\dot{\gamma}_1}$ and $\omega_{d_2}^{\dot{\gamma}_2}$ represent the angular velocity of link d_2 under the influence of the wing first and second section, respectively. In order to find the contribution of $\omega_{d_2}^{\dot{\gamma}_1}$, which is the angular velocity due to the flapping of the wing first section, it is sufficient to draw the velocity of the wing first section end at B_2 location, and find the center of rotation on the basis of it. In order to find the instantaneous center of rotation which is obtained by intersecting directions perpendicular to $\vec{V}_{A_2}$ and $\vec{V}_{B_2}$ velocities, the equations of line III and IV are derived as follows:

$$y - y_{B_2} = (x + x_{B_2}) \tan \gamma_1 \tag{17}$$

$$y = x \tan \lambda_2 \tag{18}$$

$$B_2 = \begin{bmatrix} -e + L_1 \cos \gamma_1 + l_2 \cos \gamma_2 \\ h + L_1 \sin \gamma_1 + l_2 \sin \gamma_2 \end{bmatrix} \tag{19}$$

In the above equations x_{B_2} and y_{B_2} are the coordinates of point B_2. Equation (17) is the equation of the line which B_2 is one of its points and $\tan \gamma_1$ is its slope. Moreover, Eq. (18) represents the line passing through A_2, which center of coordinate is one of its points and $\tan \lambda_2$ is its slope. The intersection of these two lines, one can get the instantaneous center of rotation as follows:

$$\omega_{d_2}^{\dot{\gamma}_1} = \left(\frac{1}{\sqrt{x_{cr_1}^2 + y_{cr_1}^2} - r_2} \right) r_2 \dot{\lambda}_2 \tag{20}$$

Similarly, in order to describe the distribution of $\omega_{d_2}^{\dot{\gamma}_2}$, one can calculate $\omega_{d_2}^{\dot{\gamma}_2}$ by finding the instantaneous center of rotation by intersecting the line with slope of $\tan \gamma_2$ which passes through point B_2, and the line passes through point A_2 that the center of coordinate is one of its points and its slope is $\tan \lambda_2$:

$$y - y_{B_2} = (x + x_{B_2}) \tan \gamma_2 \tag{21}$$

$$y = x \tan \lambda_2 \tag{22}$$

$$\omega_{d_2}^{\dot{\gamma}_2} = \left(\frac{1}{\sqrt{x_{cr_2}^2 + y_{cr_2}^2} - r_2} \right) r_2 \dot{\lambda}_2 \tag{23}$$

$$\omega_{d_2} = \left(\frac{1}{\sqrt{x_{cr_1}^2 + y_{cr_1}^2} - r_2} \right) r_2 \dot{\lambda}_2$$
$$+ \left(\frac{1}{\sqrt{x_{cr_2}^2 + y_{cr_2}^2} - r_2} \right) r_2 \dot{\lambda}_2 \tag{24}$$

2.2 Main body, the power generation components and the control systems

The main body along with the power generation components and the control systems of the flapping mechanism can be modeled as a rigid body that has the translational and rotational movements in a three-

dimensional space. To construct the corresponding bond graph of each subsystem, a body fixed coordinate axis that originates at the center of mass of the body, and its axes coincide with the main axis of the body is applied. According to Fig. 2, the angular and linear kinematic parameters of the body can be decomposed along the proposed coordinate axis.

Using Newton's second law, the rotational and transitional relations can be extracted in the following way [30]:

$$\boldsymbol{F} = \left. \frac{\partial \boldsymbol{p}}{\partial t} \right|_{rel} + \boldsymbol{\omega} \times \boldsymbol{p} \tag{25}$$

$$\boldsymbol{\tau} = \left. \frac{\partial \boldsymbol{p_J}}{\partial t} \right|_{rel} + \boldsymbol{\omega} \times \boldsymbol{p_J} \tag{26}$$

In the above equations $\boldsymbol{F} = [F_x, F_y, F_z]^T$ and $\boldsymbol{\tau} = [\tau_x, \tau_y, \tau_z]^T$, respectively are the vectors of net force and torque acting on the body. Moreover, $\boldsymbol{p} = [p_x, p_y, p_z]^T$ and $\boldsymbol{p_J} = [p_{Jx}, p_{Jy}, p_{Jz}]^T$, respectively are the linear and angular momentum vectors, $\boldsymbol{\omega} = [\omega_x, \omega_y, \omega_z]^T$ is the angular velocity vector, and t represents the time. Using the results of Eqs. (25) and (26), finally, the nonlinear Euler equations of the main body are obtained as follows:

$$\dot{\boldsymbol{p}} = \boldsymbol{F} + m\boldsymbol{\omega}^T \boldsymbol{A} - m\boldsymbol{\omega}^T \boldsymbol{A}^T \tag{27}$$

$$\dot{\boldsymbol{p}_J} = \boldsymbol{\tau} + (\boldsymbol{\omega}^T \boldsymbol{J}) \boldsymbol{B}^T - (\boldsymbol{\omega}^T \boldsymbol{J}) \boldsymbol{B} \tag{28}$$
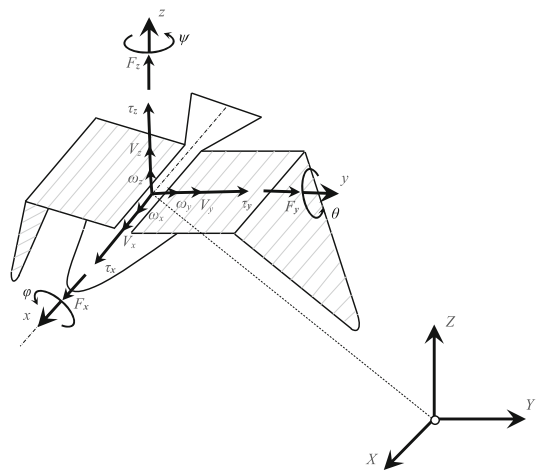
where

Fig. 2 The flapping bird in three-dimensional overall motion

$$A = \begin{bmatrix} 0 & p_z/m & 0 \\ 0 & 0 & p_x/m \\ p_y/m & 0 & 0 \end{bmatrix} \quad (29)$$

$$B = \begin{bmatrix} 0 & p_{Jz}/J_z & 0 \\ 0 & 0 & pJ_x/J_x \\ p_{Jy}/J_y & 0 & 0 \end{bmatrix} \quad (30)$$

J is the diagonal matrix of J_x, J_y and J_z the mass moments of inertias, and m represents the body mass. Solving the Euler equations, the values of the linear velocities V_x, V_y and V_z, as well as the angular velocities ω_x, ω_y and ω_z are obtained relative to the coordinate system, which continuously changes the principle directions, it would be difficult to interpret the body motion with respect to the body-fixed coordinates. Moreover, in order to use the Euler equations, the components of the external forces and torques (derived from the coordinate system connected to the body) should be aligned with the coordinate axes connected to the body. Since it is unlikely that the external forces and moments will be easily linked to continuously changing directions, and since the interpretation of body movements with respect to the body-fixed coordinates is difficult, so it is necessary to look for a coordinate transformation from the body-fixed frame to the other more convenient frame. It could facilitate the interpretation of the motion. There are several methods of coordinate transformations that can be used to transfer the body-fixed coordinates to the inertial coordinates, but among them, the most popular one is using the Euler angles φ (roll), θ (pitch) and ψ (yaw). Accordingly, the corresponding transformation matrices are defined as follows:

$$\Phi = \begin{bmatrix} 1 & 0 & 0 \\ 0 & \cos\phi & -\sin\phi \\ 0 & \sin\phi & \cos\phi \end{bmatrix} \quad (31)$$

$$\Theta = \begin{bmatrix} \cos\theta & 0 & \sin\theta \\ 0 & 1 & 0 \\ -\sin\theta & 0 & \cos\theta \end{bmatrix} \quad (32)$$

$$\Psi = \begin{bmatrix} \cos\psi & -\sin\psi & 0 \\ \sin\psi & \cos\psi & 0 \\ 0 & 0 & 1 \end{bmatrix} \quad (33)$$

Now, having the linear and angular velocities of the bird in the body-fixed coordinates system, the corresponding components of these velocities can be determined in the inertial coordinates system. Accordingly, using the following rotation matrices, the transformation from the body-fixed coordinates to the inertia coordinates is done:

$$V_{XYZ} = \Psi\Theta\Phi V \quad (34)$$

$$\omega_{XYZ} = \Psi\Theta\Phi\omega \quad (35)$$

In the above equations, $V = [V_x, V_y, V_z]^T$ is the bird linear velocity vector in the body-fixed frame, $V_{XYZ} = [V_X, V_Y, V_Z]^T$ is the bird linear velocity vector in the inertial frame and $\omega_{XYZ} = [\omega_X, \omega_Y, \omega_Z]^T$ is the bird angular velocity vector in the inertial frame. In order to transform the coordinate axes, the Euler angles φ, θ and ψ are required which can be calculated from the following equation:

$$\omega = \begin{bmatrix} \dot\phi - \dot\psi\sin\theta \\ \dot\theta\cos\phi + \dot\psi\cos\theta\sin\phi \\ -\dot\theta\sin\phi + \dot\psi\cos\theta\cos\phi \end{bmatrix} \quad (36)$$

Solving the above equations, $\dot\theta$, $\dot\psi$ and $\dot\phi$ are obtained as follows:

$$\begin{bmatrix} \dot\theta \\ \dot\psi \\ \dot\phi \end{bmatrix} = \begin{bmatrix} \cos\phi\,\omega_y - \sin\phi\,\omega_z \\ \dfrac{\sin\phi}{\cos\theta}\omega_y + \dfrac{\cos\phi}{\cos\theta}\omega_z \\ \omega_x + \sin\phi\dfrac{\sin\theta}{\cos\theta}\omega_y + \cos\phi\dfrac{\sin\theta}{\cos\theta}\omega_z \end{bmatrix} \quad (37)$$

Finally, integrating the above relations, φ, θ and ψ are obtained that are the modulated variables, and their initial values are considered to be zero.

2.3 Articulated flapping wing, considering the effects of the aerodynamic and torsional forces

In the present model, the articulated wings are considered for the flapping bird. The main motivation for utilizing the articulated wings is the ability of the wing root in producing the lift force, and the wing tip in producing the thrust force. As a result, the wing first-section lacks a twisting mechanism, and only the second-section has a twisting mechanism. Here, the flapping mechanism of the wing both sections is considered independently.

2.3.1 Governing kinematic equations of the articulated wing

In the field of the kinematic science, position, velocity, acceleration, and all higher derivatives of the space variables (relative to time or any other variables) are investigated, and accordingly, the kinematics of the connected mechanical robotic manipulators contains all of the geometric and the time dependent features of the motion. In order to extract these kinematic equations, the location and orientation of the connected links are investigated. In order to simplify the study of their movement, the frames are connected to the link joints according to the Fig. 3. The lengths of the first and second sections of the wing are respectively L_1 and L_2, and the flapping angles of each section around their respective axes are γ_1 and γ_2 respectively. The wing first section has the constant chord of $c_{1,i=1,\ldots,5} = 0.2$, and the second section has the variable chord of $c_{2,i=2,4,\ldots,10} = c_{2,i=1,3,\ldots,9} = (0.2, 0.25, 0.2, 0.15, 0.1)$.

According to Fig. 3:

$$\boldsymbol{r_1} = \begin{bmatrix} s_1 \cos \gamma_1 \\ s_1 \sin \gamma_1 \end{bmatrix} \tag{38}$$

$$\boldsymbol{v_1} = \begin{bmatrix} -s_1 \dot{\gamma}_1 \sin \gamma_1 \\ s_1 \dot{\gamma}_1 \cos \gamma_1 \end{bmatrix} \tag{39}$$

$$\boldsymbol{r_2} = \begin{bmatrix} L_1 \cos \gamma_1 + s_2 \cos(\gamma_1 + \gamma_2) \\ L_1 \sin \gamma_1 + s_2 \sin(\gamma_1 + \gamma_2) \end{bmatrix} \tag{40}$$
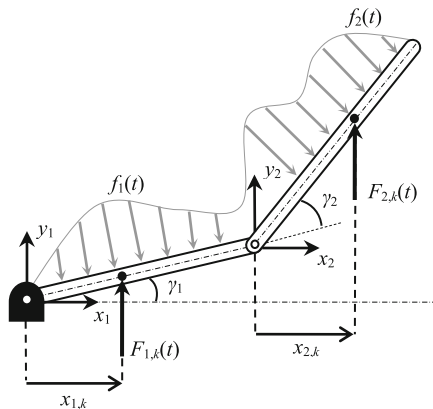

Fig. 3 Kinematic details of the present two-section wing

$$\boldsymbol{v_2} = \begin{bmatrix} -L_1 \dot{\gamma}_1 \sin \gamma_1 - s_2(\dot{\gamma}_1 + \dot{\gamma}_2) \sin(\gamma_1 + \gamma_2) \\ L_1 \dot{\gamma}_1 \cos \gamma_1 + s_2(\dot{\gamma}_1 + \dot{\gamma}_2) \cos(\gamma_1 + \gamma_2) \end{bmatrix} \tag{41}$$

In which, $\boldsymbol{r_1} = [x_1, y_1]^T$ and $\boldsymbol{r_2} = [x_2, y_2]^T$ represents the position vector of each proposed point of the first and the second sections of the wing relative to the origin of the coordinates attached to their joint. $\boldsymbol{v_1} = [v_{x,1}, v_{y,1}]^T$ and $\boldsymbol{v_2} = [v_{x,2}, v_{y,2}]^T$ are the corresponding velocity vectors at those points, and s_1 and s_2 are measured along the span length relative to the origin of the first and the second sections, respectively.

2.3.2 Wing aerodynamic model considering the torsion and the body angle of attack

In the present model, the effect of aerodynamic forces on the wing, wing torsion, and body angle of attack are considered. The aerodynamic forces are as the distributed forces applied to the wing. Therefore, in addition to the concentrated force applied from the power transmission system, the distributed force that actually represents the aerodynamic forces on the wing, must also be taken into account. According to Fig. 3, Newton's second law for the bond graph modeling of the distributed aerodynamic forces on the wing and the concentrated forces applied by the mechanism to each sections of the wing can be present as follows:

$$\sum F = ma = \sum_{i=1}^{2} \left(\int_0^{L_i} f_i(x_i, t) dr_i + \sum_{k=1}^{n} F_{i,k}(x_{i,k}, t) \right)$$
$$k = 1, 2, \ldots, \infty \tag{42}$$

where $f_i(x_i, t)$ presents the distributed force of the wing ith section, and $F_{i,k}(x_{i,k}, t)$ represents the concentrated force which is applied from the mechanism to the wing ith section at point $x_{i,k}$, and m and a are respectively the wing mass and acceleration. It should be noted that, each wings sections of the articulated flapping wings produces the aerodynamic lift and propulsive forces separately. Ultimately, these forces are integrated along the wingspan after projection and creation of the aerodynamic forces and moments applied to the body. Based on the velocity and angle of attack of various wing elements, the calculation of the lift and the drag forces coefficients are done through the approximate

functions, and the resulting lift L_i and drag D_i forces of the wing ith section are calculated. In this regard, the angle of attack variations along the wing span can be considered as follows:

$$\alpha_i(\boldsymbol{r}_i) = \alpha_{0,i} - \tan^{-1}\left(\frac{V_z}{V_x}\right) + \tan^{-1}\left(\frac{v_{y,i}}{V_x}\right) - \varepsilon_i \quad (43)$$
$$i = 1, 2$$

In the above equation, the first term $\alpha_{0,i}$ is the initial incidence angle of ith section of the wing which is considered constant in the present modeling. The second term α_{body} represents the body angle of attack. The third term α_{wing} presents the flapping contribution in changing the angle of attack of ith section of the wing, and finally the fourth term ε_i introduces the twist angle of the ith section. This twisting angle is calculated based on the aeroelastic coupling. The details of the torsional aeroelastic model are presented in the following. In addition, $v_{y,i}$ is the linear vertical velocity of the wing ith section, V_x is the flapping wing forward velocity and V_z is the flapping bird upward velocity.

In this study, the angle of attack is calculated separately for each wing, and the integral of the aerodynamic forces are evaluated. Consequently, the wings are independent from each other, and the asymmetric analysis would be possible. The instantaneous lift force of each section of the left and the right wings can be evaluated as follows by the use of the thin airfoil theory:

$$L_i(t) = \frac{1}{2}\rho_a \int_0^{L_i} \left(V_x^2 + v_{y,i}^2 + V_z^2\right) c_{l,i}\, dS_i \quad i = 1, 2$$

$$(44)$$

In the above equation, dS_i is the cross section area of an element of the wing ith section in top view and is equal to $c_i ds_i$ in which c_i is the wing ith section chord and ρ_a is the air density. Also, $c_{l,i}$ is the lift coefficient of the wing ith section. The aerodynamic models with a range of the angle of attack variations beyond the stall should be utilized, in order to increase the accuracy of the calculation of the aerodynamic lift and drag forces coefficients, and the estimation of the coefficients under the condition of the flow separation that is inevitable for a flapping bird with the single-

section wings. Here, the experimental data related to the flat plate are used, and an appropriate curve is fitted to these data, which approximately contains two linear functions:

$$c_l = \begin{cases} a_0\alpha & \alpha \prec \alpha_{stall} \\ \left(\frac{\pi}{2} - \alpha\right)\left(\dfrac{c_{l_{stall}}}{\pi/2 - \alpha_{stall}}\right) & \alpha \geq \alpha_{stall} \end{cases} \quad (45)$$

where α_{stall} and $c_{l_{stall}}$, respectively are the stall angle of the cross section and the lift coefficient immediately after stall. a_0 is the slope of the lift curve in linear state. For estimating the drag coefficient according to the experimental data and the simple curve fit, the following pattern can be suggested:

$$C_d = \begin{cases} C_{d_{max}}\left(\dfrac{1-\cos 2\alpha}{2}\right) + C_{d_0} & \alpha \prec \alpha_{stall} \\ C_{d_{max}}\left[\left(\dfrac{1-\cos 2\alpha}{2}\right) + C_{d_0} + C_{d_{stall}}\right] & \alpha \succ \alpha_{stall} \end{cases}$$

$$(46)$$

In this equation, C_{d_0} and $C_{d_{stall}}$, respectively are the friction drag coefficient and the drag coefficient due to the flow separation. The value of $C_{d_{max}}$ for a flat plate is equal to about 2 which corresponds the angle of 90°. The above empirical factors are estimated based on the experimental data available for wind tunnel test of very thin sections. To sum up, it can be said that the application of the models, which describe the aerodynamic coefficients, makes it possible to effectively compare and indicate the relative advantages of using the two-section wings in reducing the probability of the flow separation and stall. Now, the instantaneous drag force of each section of the left and the right wing can is evaluated as:

$$D_i(t) = \frac{1}{2}\rho_a \int_0^{L_i} \left(V_x^2 + v_{y,i}^2 + V_z^2\right) C_{d,i}\, dS_i \quad i = 1, 2$$

$$(47)$$

Finally, the propulsive force component $F_{x,i}$, the vertical force component $F_{z,i}$, as well as the lateral force component $F_{y,i}$, which apply to the body from the ith section of each wing at any moment, can be evaluated from the following relationships:

$$F_{x,i}(t) = \frac{1}{2}\rho_a \int_0^{L_i} \left(V_x^2 + v_{y,i}^2 + V_z^2\right)$$

$$[c_{l,i}\sin\alpha_i - C_{d,i}\cos\alpha_i]\,dS_i \quad i = 1,2 \tag{48}$$

$$F_{z,i}(t) = \frac{1}{2}\rho_a \int_0^{L_i} \left(V_x^2 + v_{y,i}^2 + V_z^2\right)$$

$$[c_{l,i}\cos\alpha_i + C_{d,i}\sin\alpha_i]\cos\left(\sum_{j=1}^{i}\gamma_j\right)dS_i \quad i = 1,2 \tag{49}$$

$$F_{y,i}(t) = \frac{1}{2}\rho_a \int_0^{L_i} \left(V_x^2 + v_{y,i}^2 + V_z^2\right)$$

$$[c_{l,i}\cos\alpha_i + C_{d,i}\sin\alpha_i]\sin\left(\sum_{j=1}^{i}\gamma_j\right)dS_i \quad i = 1,2 \tag{50}$$

Similarly, the aerodynamic moments of the M_φ, M_θ and M_ψ applied to the body are also calculated summing up the moments produced by the wing both sections:

$$M_\phi(t) = \sum_{i=1}^{2} \int_0^{L_i} \left[F_{z,i}^L - F_{z,i}^R\right]s_i\,ds_i \tag{51}$$

$$M_\theta(t) = \sum_{i=1}^{2} \int_0^{L_i} \left[F_{z,i}^L + F_{z,i}^R\right]\left(d - \frac{c_i}{4}\right)ds_i \tag{52}$$

$$M_\psi(t) = \sum_{i=1}^{2} \int_0^{L_i} \left[F_{x,i}^L - F_{x,i}^R\right]s_i\,ds_i \tag{53}$$

where $F_{x,i}^L$ and $F_{z,i}^L$, respectively represent the propulsive and the vertical forces produced by the ith section of the left wing. Similarly, $F_{x,i}^R$ and $F_{z,i}^R$, respectively represent the propulsive and the vertical forces produced by the ith section of the right wing. d represents the distance between the leading edge and the center of mass of the whole wing which is equal to 0.02. It should be noted that, at this step the changes in the location of the wing center of mass and the moments of inertia while flapping, are not taken into account. In addition, the aerodynamic center is located at $c_i/4$ for thin airfoils at low speeds, and $c_{m_{c_i/4}} = 0$ for thin and symmetrical airfoils.

2.3.3 Aerodynamic modeling of the flapping bird tail

The lift force of the tail has two effects on the body: 1. This force is added to the vertical force of the body and then applied to it. 2. This force is multiplied by the distance between the center of mass of the tail from the wing and is added to the pitch moment. For this purpose, the model of the pitch moment results from the tail is added to the pitch moment equation as follows:

$$\alpha_{tail} = -\tan^{-1}\left(\frac{V_z}{V_x}\right) + \delta_e + \tan^{-1}\left(\frac{Ql_{tail}}{V_x}\right) \tag{54}$$

where Q is the rate of pitch, l_{tail} is the distance between the tail and the wing center of mass which is considered 0.3 m. δ_e is the deviation angle of the elevator, which is assumed to be zero. The lift force produced by the tail is evaluated by the following equation:

$$L_{tail} = \frac{1}{2}\rho_a c_{l_{max}}\left((Ql_{tail})^2 + V_x^2\right)\sin(2\alpha_{tail})S_{tail} \tag{55}$$

In the above equations, α_{tail} represents the tail angle of attack, and S_{tail} is the tail area which is considered equal to 0.008 m².

2.3.4 Torsional mode shapes of the articulated wing

The initial model has a passive (predetermined) twisting angle, the equations of which were given in the previous section. At this step, it is possible to investigate the torsional aero elastic characteristics of the wing by defining its torsional mode shapes, and considering the dynamics of the wing torsional deformations.

The beams have many features of the conventional aviation structures. The high-aspect ratio wings and the rotor blades of the helicopters are often considered ideally as the beams in preliminary designs. Even for low-aspect ratio wings, although the plate model is more realistic, the bending and the torsional deformations of the wing can be estimated using the beam theory, taking into account the adjusted torsional stiffness coefficient. At first, the non-uniform

properties will be considered for the beam along the s-axis, which is chosen to be coinciding with the elastic axis of the beam. In the beams ideal model, this axis is assumed to be straight, and in other word, it corresponds to the locus of the cross-sectional shear centers. This selection of the s-axis structurally uncouples the torsion and the transverse bending displacements for the isotropic beams. The torsional elastic deformations θ_t are positive in the direction of the right-hand side. The twisting moment T is the structural torque, which here, T represents the external aerodynamic torque, which is equal to the summation of the distributed torques on the first and the second sections of the wing, and is calculated from the following equation:

$$T(s,t) = \sum_{i=1}^{2} T_i(s_i,t) = -\sum_{i=1}^{2} \frac{c_i}{4} F_{z,i} \qquad (56)$$

Considering $\rho_b I_p ds$ as the polar mass moment of inertia about the s-axis, the equation of motion is determined by equating the resultant twisting moment on both ends of the integrated element to the rate of change of the element angular momentum about the elastic axis:

$$\frac{\partial T}{\partial s} = \rho_b I_p \frac{\partial^2 \theta_t}{\partial t^2} \qquad (57)$$

where

$$\rho_b I_p = \int_A \rho_b \left(y^2 + z^2\right) dA \qquad (58)$$

In this case, A is the transverse cross sectional area of the beam, y and z are the Cartesian coordinates of the transverse cross section, and ρ_b is the mass density of the beam. As long as ρ_b of the cross section is constant, I_p is the area of the polar mass moment of inertia per unit length. However, when ρ_b changes along the cross-section of the beam, $\rho_b I_p$ is interpreted as mass polar moment of inertia for the cross-section. The twisting moment can be written in terms of the twist rate and the Saint–Venant torsional rigidity as follows:

$$T = GJ \frac{\partial \theta_t}{\partial s} \qquad (59)$$

Putting this equation in Eq. (56), the partial differential equation of motion for a non-uniform beam is obtained as follows:

$$\frac{\partial}{\partial s}\left(GJ \frac{\partial \theta_t}{\partial s}\right) = \rho_b I_p \frac{\partial^2 \theta_t}{\partial t^2} \qquad (60)$$

For the special case of the uniform beams, this equation simplifies to the one-dimensional wave equation as follows:

$$\frac{GJ}{\rho_b I_p} \frac{\partial^2 \theta_t}{\partial s^2} = \frac{\partial^2 \theta_t}{\partial t^2} \qquad (61)$$

Taking into account the distributed torques on the wing surface, the above equation occurs in the following form:

$$\rho_b I_p \frac{\partial^2 \theta_t}{\partial t^2} - GJ \frac{\partial^2 \theta_t}{\partial s^2} = \int_0^L T(s,t)\varphi_t(s)\,ds \qquad (62)$$

where φ_t presents the torsional mode shapes. In order to calculate the torsional mode shapes, the homogeneous solution of the above equation is used. Using the separation of variables method, and taking into account the boundary conditions of the two ends of the beam (clamped end at $s = 0$ and free end at $s = L$), the modal stiffness α_j and natural frequencies ω_j are respectively obtained as follows:

$$\alpha_j L = \frac{(2j-1)\pi}{2} \quad j = 1,2,\dots \qquad (63)$$

$$\omega_j = \alpha_j \sqrt{\frac{GJ}{\rho_b I_p}} = \frac{(2j-1)\pi}{2L} \sqrt{\frac{GJ}{\rho_b I_p}} \quad j = 1,2,\dots \qquad (64)$$

In addition, the mode shapes or the eigenfunctions are obtained from the following equation:

$$\varphi_{t,j}(s) = \sin(\alpha_j s) = \sin\left[\frac{(2j-1)\pi s}{2L}\right] \quad j = 1,2,\dots \qquad (65)$$

Finally, the non-homogeneous solution of Eq. (44) results in the following relation, based on which the bond graph model of the wing torsion is constructed:

$$\rho_b I_p \ddot{Y}(t) + GJ \alpha_j^2 Y(t) = \int_0^L T(s,t)\varphi_{t,j}(s)\,ds \qquad (66)$$

where $Y(t)$ is the time respons.

2.3.5 Aerodynamic power and propulsive efficiency

The performance quantities including power and efficiency, which are criteria for evaluating bird aerodynamic performance, are averaged and calculated using the following relationships in one cycle within the steady oscillatory interval:

$$P_{in,steady}^A = \frac{1}{T} \int_0^T M\omega \, dt \qquad (67)$$

In the above relation, $P_{in,steady}^A$ is the average input power which is actually the power consumed in the flapping mechanism. T is the flapping period and ω is the flapping instantaneous angular velocity, which can equivalent to any of the angular velocities of the first and second sections of the wing i.e. $\dot{\gamma}_1$ and $\dot{\gamma}_2$.

Moreover, M is the aerodynamic bending moment of the wing hinge-point which is evaluated from the following equation:

$$M = \frac{1}{2} \rho_a \sum_{i=1}^2 \int_0^{L_i} \left(V_x^2 + v_{y,i} + V_z^2 \right) c_i c_{l,i} s_i \, ds_i \qquad (68)$$

Finally, the propulsive efficiency η can be obtained as follows:

$$\eta = \frac{P_{out,steady}^A}{P_{in,steady}^A} \qquad (69)$$

where $P_{out,steady}^A$ is the average useful power:

$$P_{out,steady}^A = \frac{1}{T} \int_0^T F_x V_x \, dt \qquad (70)$$

3 Bond graph model of the flapping wing

The complete bond graph model of the system can be constructed from the combination of the bond graph of its subsystems. In order to simplify, the comprehensive bond graph of the present system can be developed, considering its subsystems as follows: 1. A pair of the separated power system for each wing, including two DC motors and two mechanisms that produce the flapping motions for each wing section independently. 2. Main body and its accessories, and

the forces and moments transmitted to it. 3. Two-section wings, considering its aerodynamic model and the elastic torsion. 4. Tail.

In bond graph environment, the basic concept is to determine the flow of energy in a system. In any sort of systems, the energy flow is always directed by simultaneous involvement of two independent parameters. These two parameters are defined by the general power variables of Effort e and Flow f. So, the language of bond graphs aims to represent the physical systems through power interactions. These power factors have different explanations in different physical domains. However, in several energy domains, power could always be utilized as a generalized coordinate to model coupled systems. One of these systems might be an electrical motor driving a crank; in which the form of energy varies in the system. Fore more clarity, in Table 1, the power (effort and flow) and energy variables of different parts of the present model are listed.

Figure 4 indicates the bond graph model of the flapping bird power system. The DC motor is an electromechanical system. The motor armature has a resistance and an inductance that converts the electrical energy to the mechanical one. The motor model consisting of a source of effort is connected to the 1-junction and the gyrator. The 1-junction represents the constant flow passing through the armature, and the inductance and the resistance bonds are connected to it. The gyrator essentially acts as the energy converter from electrical to mechanical one, and is connected to the 1-junction which represents the angular velocity of the motor shaft. It should be noted that the core of the motor bond graph model is its GY, which represents the propulsive force generated by the electrical energy. In addition, the input voltage is modeled as the source of effort (Se) in the bond graph. The small gear mount on the motor shaft is connected to the crank (Fig. 1), and in fact, the source of flow is a velocity that comes from the DC motor, and is considered as an input to produce the angular motion of the crank. It is presented as a 1-junction with an I-element that expresses the rotational inertia of the crank around its own axis. The bond graph of the flapping mechanism of the wings is constructed of 1-junctions related to the rotational velocities of the cranks, the flapping velocities, and the linear and angular velocities of the connecting rods center of mass, which are connected to I-elements represented

Table 1 Power and energy variables in various energy domains of the present model

| Energy domains of the subsystems		Power variables		State variables		Power	Energy
		Effort	Flow	Generalized displacement (q)	Generalized momentum (p)		
Wing	Mechanical translation	Force (F)	Velocity (V)	Displacemen (s)	Momentum (p)	$F(t)V(t)$	$\int\limits^{s} Fds; \int\limits^{p} Vdp$
	Mechanical rotation	Torque (T)	Angular velocity ($\dot{\gamma}$)	Angle (γ)	Angular momentum (p_J)	$T(t)\dot{\gamma}(t)$	$\int\limits^{\gamma} Td\gamma; \int\limits^{p_J} \dot{\gamma}dp_J$
Power system	Electrical	Voltage (E_a)	Current (I_a)	Charge (q)	Flux linkage (λ)	$I_a(t)E_a(t)$	$\int\limits^{q} E_a dq; \int\limits^{\lambda} I_a d\lambda$
	Mechanical translation	Force (F)	Velocity (V)	Displacement (r)	Momentum (p)	$F(t)V(t)$	$\int\limits^{r} Fdr; \int\limits^{p} Vdp$
	Mechanical rotation	Torque (τ)	Angular velocity ($\dot{\lambda}$)	Angle (λ)	Angular momentum (p_J)	$\tau(t)\dot{\lambda}(t)$	$\int\limits^{\lambda} \tau d\lambda; \int\limits^{p_J} \dot{\lambda}dp_J$
Body	Mechanical translation	Force (F)	Velocity (V)	Displacement (x)	Momentum (p)	$F(t)V(t)$	$\int\limits^{x} Fdx; \int\limits^{p} Vdp$
	Mechanical rotation	Torque (τ)	Angular velocity (ω)	Angle ($E \equiv \varphi, \theta, \psi$)	Angular momentum (p_J)	$\tau(t)\omega(t)$	$\int\limits^{E} \tau dE; \int\limits^{p_J} \omega dp_J$
Tail	Mechanical rotation	Torque (τ)	Angular velocity (ω)	Angle (θ)	Angular momentum (p_J)	$\tau(t)\omega(t)$	$\int\limits^{\theta} \tau d\theta; \int\limits^{p_J} \omega dp_J$

the mass and the moment of inertia of the components of the mechanism. The Modulated Transformers (MTF) relate these 1-junctions to each other. The modules of the transformers have been derived from relations (4), (5), (11), (14), (15) and (24).

In Fig. 5, the main body bond graph along with the horizontal, vertical and the lateral forces, as well as the roll, pitch and the yaw moments transmitted from the wings are presented. The rigid body bond graph is modeled as the two separated triangles in which the 1-junctions are located at their vertices. One triangle expresses the linear motion and the other one represents an angular motion, also the 1-junctions at their vertices represent the linear velocities of the center of mass and the angular velocities of the body. The triangles edges, which connect the two adjacent 1-junctions, are replaced by the MGY, which the modules are the linear or the angular momentums. Also, the inertial elements (I) corresponding to the masses and the mass moments of inertias are connected to their corresponding 1-junction with the integral causality. Here, the component of the body propulsive force is generated by Eq. (48), and transmitted to the 1-junction of the linear velocity along the

body x-axis. Also, by using Eq. (49), the component of the vertical force applied to the body is generated, and is transmitted to the 1-junction of the body linear velocity along the z-axis. Finally, the body lateral force component is constructed according to Eq. (50), and is transferred to the 1-junction of the body lateral velocity along the y-axis. In the case of the moments, from Eqs. (51), (52) and (53), respectively, the roll, pitch and the yaw moments are calculated, and are applied to the 1-junctions correspond to the angular velocities along the x, y and z body-axes.

Figure 6 shows the bond graph of the body angular and linear velocites transformation from the body to the inertial coordinate system. The modulated Transformers (MTF) represent the **ΨΘΦ** transformations, which take the components of the linear and angular velocity vectors through the intermediate frames, and produce the inertial linear and angular velocities components. Finally, the bond graph of these transformations is connected to the rigid body bond graph, and makes it possible to formulate and completely present the equations of motion of the three-dimensional rigid body dynamic state equations of the rigid body. Also, according to Eq. (37), which results in the

Fig. 4 Bond graph model
of the power system
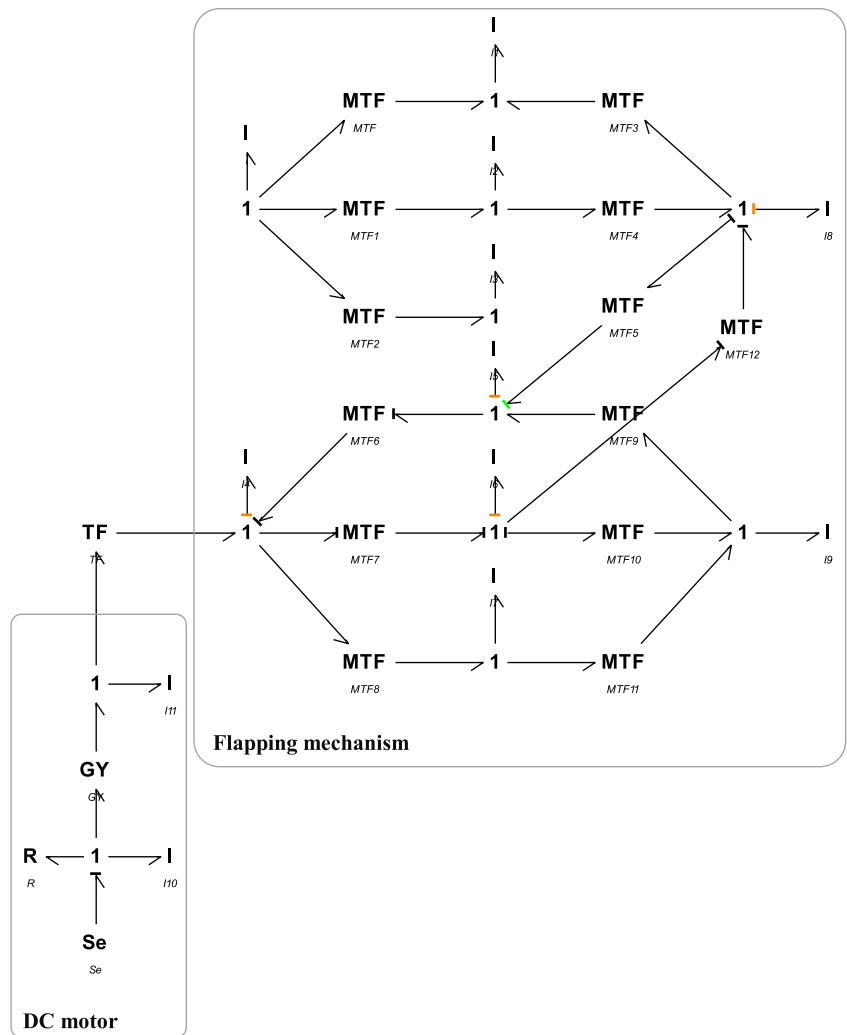
three extra state-equations, the bond graph of the generated velocities $\dot{\phi}$, $\dot{\theta}$ and $\dot{\psi}$ is indicated, and by integrating the corresponding 1-junctions, the values of the angles φ, θ and ψ can be obtained.

The bond graph of the flapping bird tail is shown in Fig. 7, which is made according to the extracted equations of the tail. Finally, the tail lift force obtained from Eq. (55) is added to the F_z force generated by the wing, and applied to the 1-junction of the body linear velocity V_z. In addition, this tail lift is multiplied to the distance between the tail and the wing center of mass $l_{tail} = 0.3(-L_{tail} \times l_{tail})$, then it is added to the pitch moment, and applied to the 1-junction of the body angular velocity ω_z.

Figure 8 presents the bond graph of the two-section flapping wing of the present bird, which is prepared based on Eqs. (39) and (41). As can be seen in this figure, Fcr_1 and Fcr_2 are the concentrated forces acting on both wing sections from the mechanism links which are connected to them, and are applied to a pair of the flapping angular velocities 1-junctions as an input to produce the flapping motion of the wing. The modal forces of the wing each section is constructed by integrating the distributed forces (lift force) on the wing [according to Eq. (42)]. The modal forces are connected to the 1-junctions presenting the wing linear velocities Vp_1 and Vp_2 through the modulated source of effort (MSe). The modules of the modulated
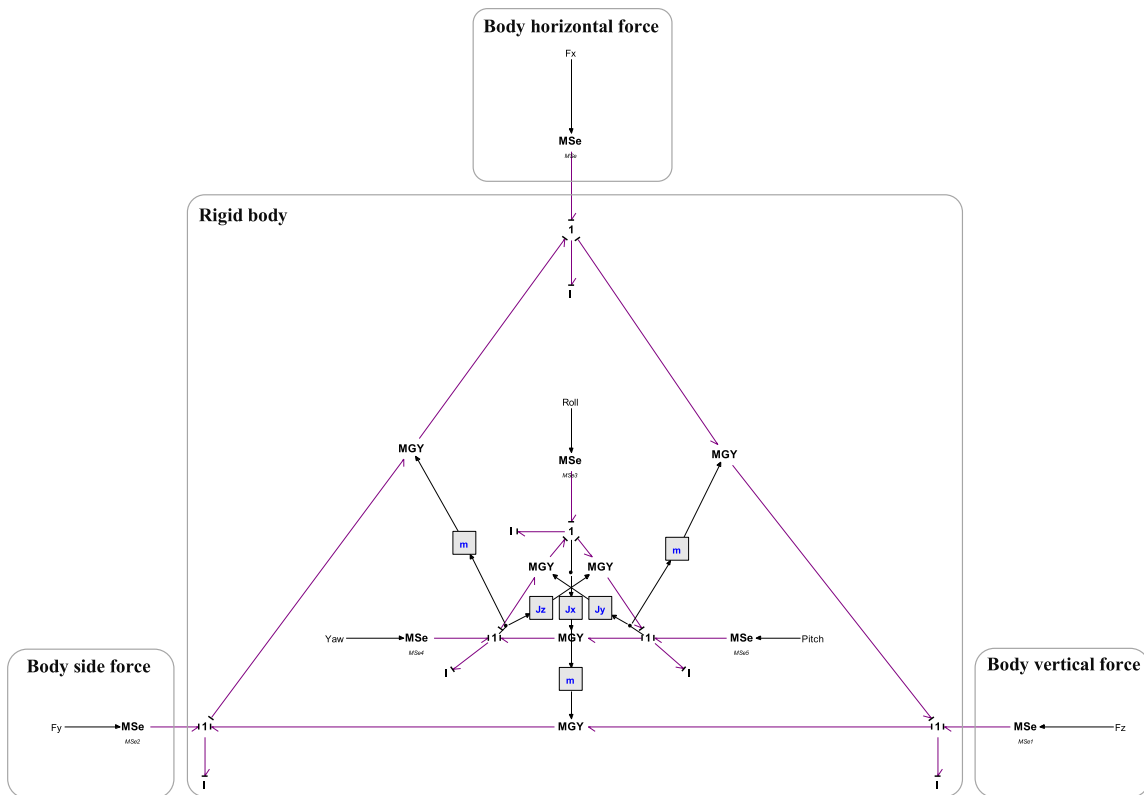
Fig. 5 Bond graph model of the main body including the forces and torques applied from the wing

transformers are embedded from the kinematic relations (39) and (41).

Figure 9 depicts the related bond graph to the torsional mode shapes of the wings, which is constructed according to relation (66). As can be observed in the figure, three torsional modes have been considered for the wing. The modulus of transformers, which are equal to the torsional mode shapes have been calculated from Eq. (65). T is obtained from Eq. (56), and T_{wing} is the wing elastic torsion, which is equal to the summation of the torsional mode shapes of the wing.

Figure 10 indicates the way of producing the aerodynamic lift and drag forces of the wing both sections, illustrating them in the coordinate planes, and generating the forces and moments transmitted from the wings to the body. Vp_1 and Vp_2 are the linear velocities of the wing first and second sections, V_x and V_z are the bird vertical and horizontal velocities, and T_W is the wing torsional torque, which construct the inputs of the aerodynamic block. Finally, F_x, F_y and F_z forces, M_φ, M_θ and M_ψ moments, and the

aerodynamic torsion distribution on the wing T constitute the outputs of the aerodynamic block.

Ultimately, the comprehensive bond graph model of the flapping bird including the main body, a pair of the flapping mechanisms, a pair of the direct current motors and two-section articulated wings considering the distribution of the aerodynamic forces on them, elastic torsion along the wing and forces and moments applied to the body is shown in Fig. 11. An important point in this bond graph is the relationship between the wing and the body. The body determines the position of the wing via defining the location of the hinge points, while the aerodynamic forces providing by the wings are applied to body, which derives the bird velocity and displacement. In other words, there are interring connections between the wings and body for transmitting linear and angular positions and aerodynamic forces and moments produced by wings flapping motion.
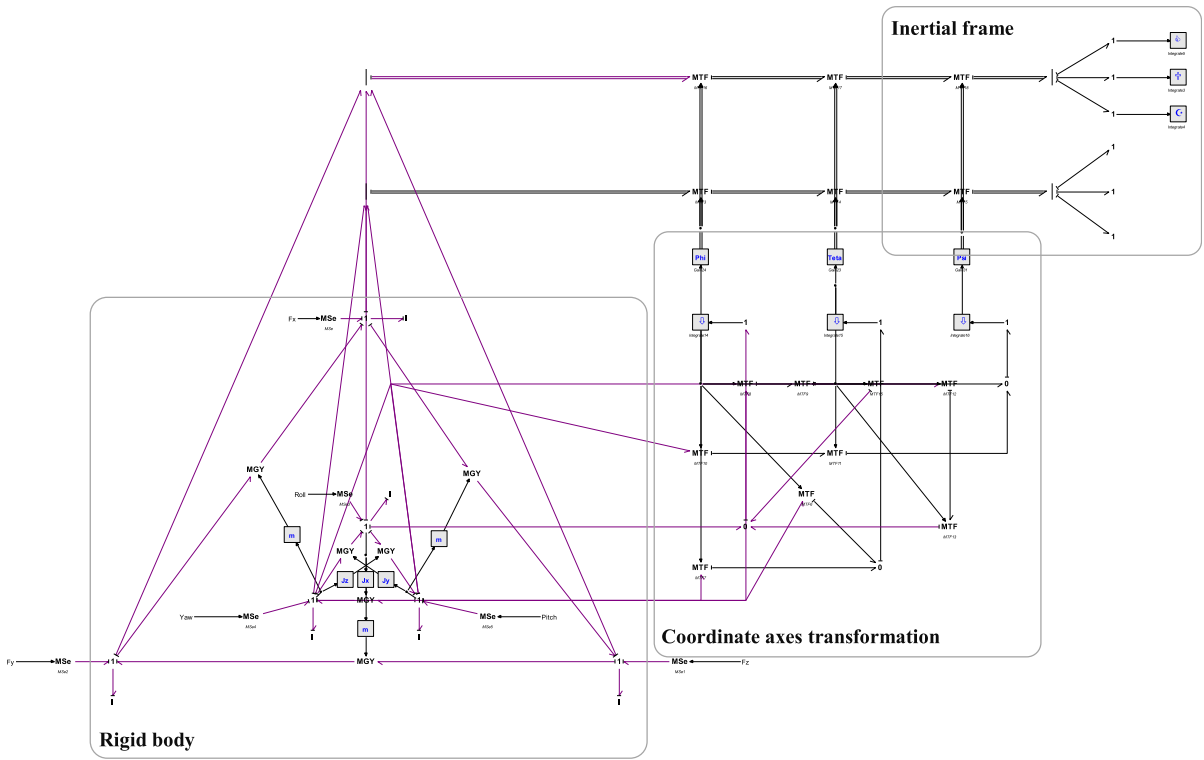
Fig. 6 Rigid body bond graph along with the coordinate transformation from the body to the inertia coordinate system
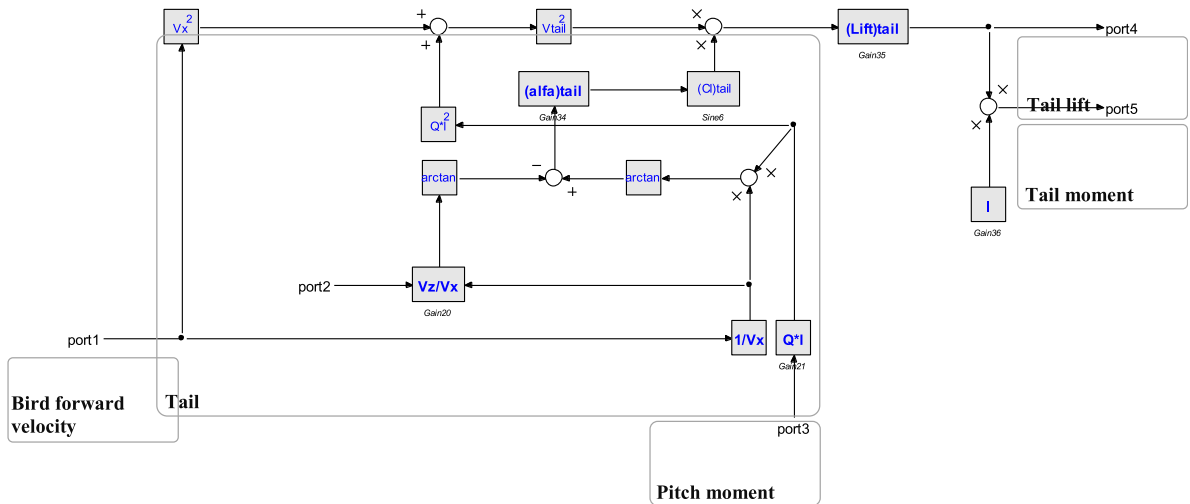

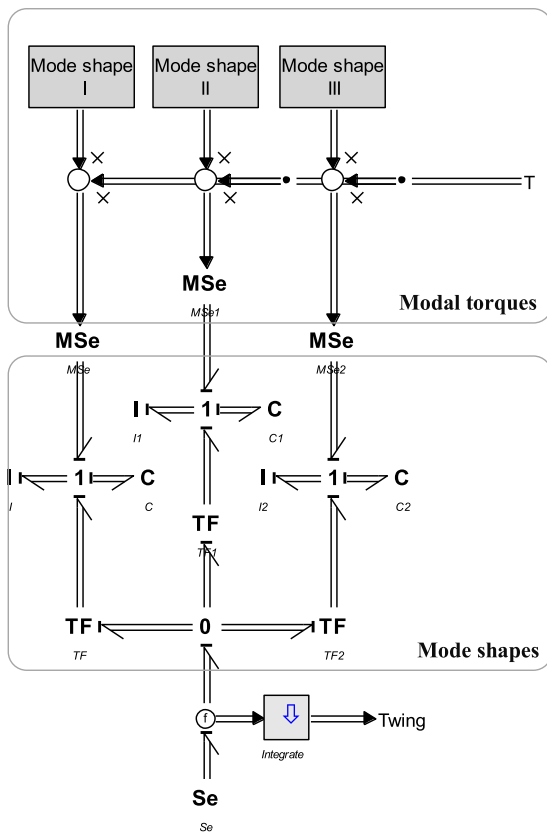Fig. 7 Bond graph model of the flapping bird tail

Fig. 8 Bond graph model
of the two-section flapping
wing considering the
distributed aerodynamic
forces on the wing

4 Results and discussion

4.1 Results validation

The present results were validated for two different
cases of typical flapping wing micro-air-vehicles
characteristics. In the first validation test case, the
verification was performed for a single-section flap-
ping wing at two constant forward velocities of 6 and
8 m/s and two initial incidence angles of 0° and 5°. In
this regard, the time-dependent variations of vertical
and forward forces of the bird at frequency of 5 Hz
were compared with the results obtained from the
MATLAB code validated by experimental data of
Pourtakdoust and Karimian [31]. This validation and
verification can be found in [29].

In the second validation case, the accuracy of the
present bond graph model in evaluating the kinematic
of the articulated flapping wing is confirmed by
comparing the velocity and displacement of the two-
section wing with the analytical solution. In Fig. 12,
the results of the present bond graph model are

compared with the results of a MATLAB code that
performs the numerical solutions by analytical
method. Generally, the results confirm the validity of
the present bond graph model, although there are few
differences. In Fig. 12a, a comparison of the flapping
angle profile for the first and second sections of the
wing can be observed. It should be noted that in the
bond graph modeling approach, the 4-bar mechanism
is developed focusing on the calculation of the
instantaneous velocities and the relationships between
the quantities. Thus, it can be expected that the
modeling approach in the bond graph environment is
different from the analytical solution approach based
on the direct insertion of the angular profiles. This
difference, and in particular the approximation of the
flapping angle to be completely harmonic, caused a
relative error about 4%. However, this error is mainly
because of a slight error in adjusting the wing
frequency due to the use of a descriptive function to
calculate the frequency in terms of the motor voltage.
In Fig. 12b, the comparison between the angular
velocities of the first and second sections of the wing is

Fig. 9 Bond graph model of the torsion block includes the torsional mode shapes of the wing

shown. As can be seen, the angular velocity amplitude obtained from the bond graph model has an acceptable accuracy level. A comparison between the instantaneous linear velocity and displacement of the end points of the wing first and second sections with the numerical data is indicated in Fig. 12c, d, respectively. Since the angular velocity and flapping angle profiles obtained from the bond graph model have relatively high conformity with the analytical solution, so, the same adaptations can be seen for these quantities.

4.2 Performance of the two-section flapping wing

In this section, the results of the bond graph model are presented to investigate the flying performance of the two-section flapping bird. In Fig. 13, the results of the aerodynamic modeling in the nominal conditions are indicated for the forward velocity of 6 m/s, the initial wing incidence angle of zero, the flapping frequency of 6 Hz, the wing both sections flapping amplitude of 30°, and the phase difference between the both wings sections of 180°. The results are presented for one flapping cycle according to the γ-t pattern shown in Fig. 13. As it is observed and expected, the average vertical force F_z is zero, since the wing incidence angle is zero, and the aeroelastic behavior is symmetric. In the same situation, the horizontal force F_x indicates a positive average value. Based on a simple distribution of the plunging motion, it would be possible to predict the propulsive force in symmetric flapping condition.
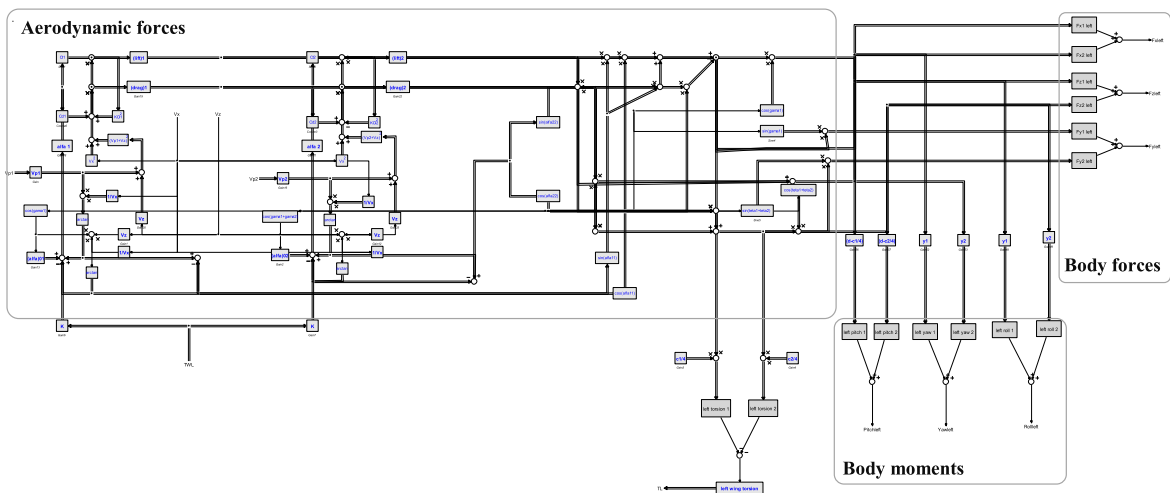
Fig. 10 Bond graph of the aerodynamic block including the aerodynamic forces and their transformations
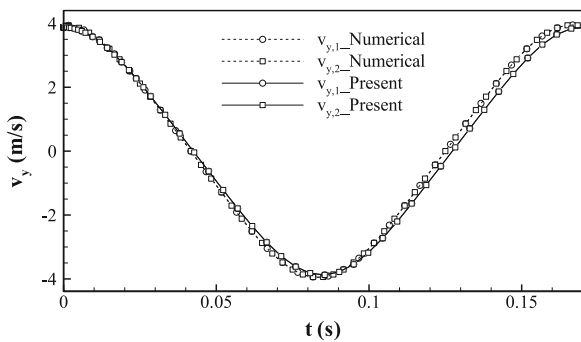
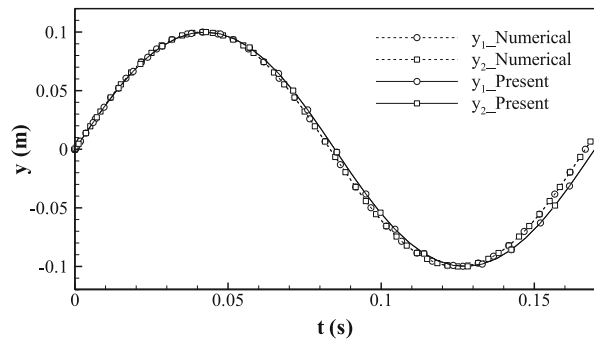**Fig. 11** The comprehensive bond graph model of the flapping bird
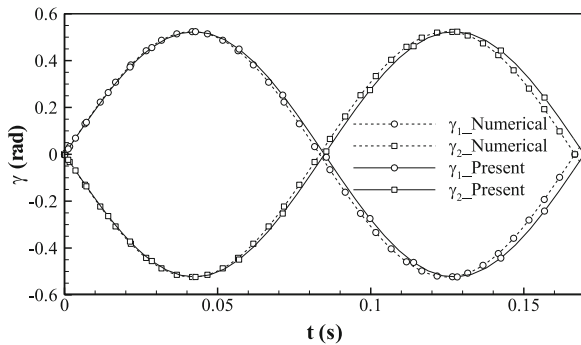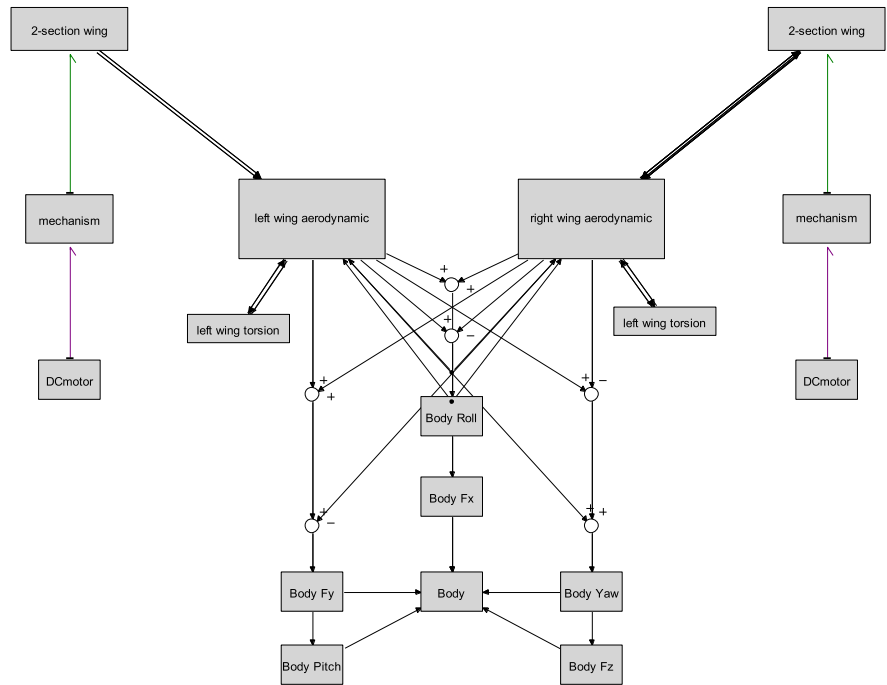
(a)
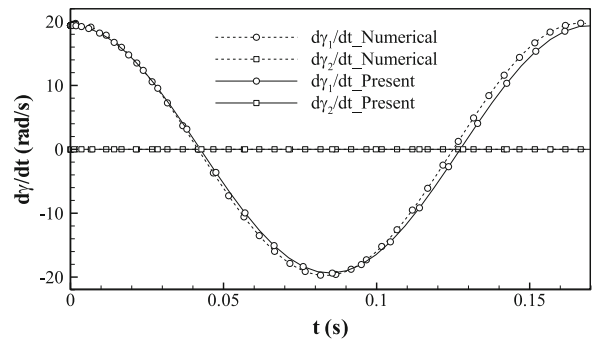
(b)

(c)

(d)

Fig. 12 Comparison between the bond graph model and the analytical solution results. **a** flapping angles of the wing first and second sections, **b** angular velocities of the wing first and second sections, **c** vertical linear velocities of the end points of the wing first and second sections, and **d** vertical displacement of the end points of the wing first and second sections

Fig. 13 Variations of the
propulsive force, vertical
force, pitch moment,
flapping angles, consumed
power, useful power, wing
tip angle of attack, and the
wing tip twist angle versus
time in nominal conditions
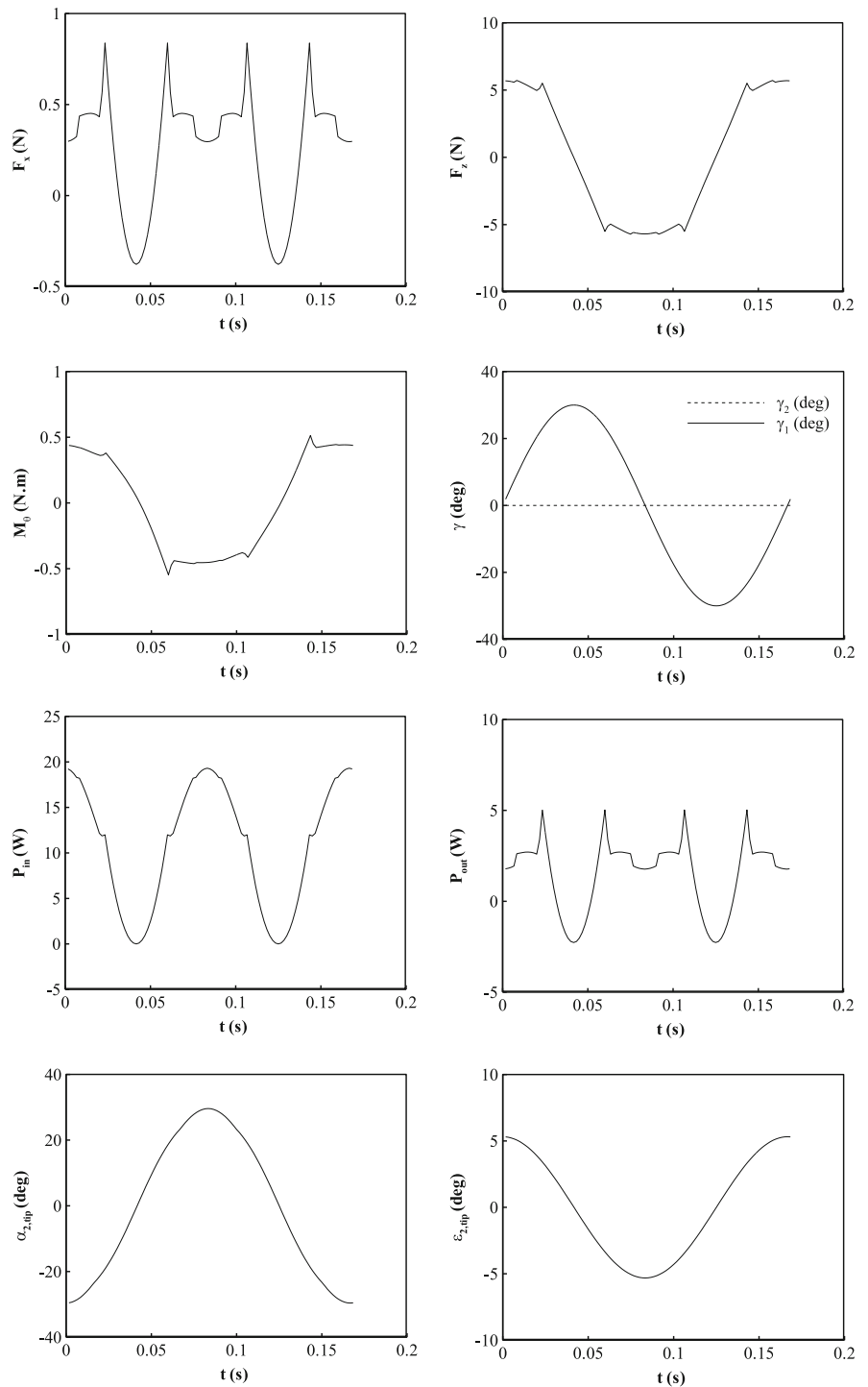
An interesting point is the dominant frequency of the horizontal force which is usually twice the flapping frequency. In the ideal condition, the horizontal force curve has positive value. There are two reasons for

existence of some intervals in which the horizontal force becomes negative. First, the torsional stiffness is such that the variations of angle of attack due to the summation of the total aerodynamic and inertial forces

are more than its initial values. As a result, in some regions of the wing, the sign of the resultant aerodynamic force changes. Second, in aerodynamic modeling of the drag force, descriptive functions were utilized to increase the force at the high angles of attack. As expected, the generated propulsive power P_{out} has the same pattern as well as the propulsive force, and in some time periods, the useful propulsive power is negative. In order to provide a criterion for the range of variations of the important angles in the flapping motion, the wing tip angle of attack $\alpha_{2,tip}$ and the elastic torsion of the wing tip $\varepsilon_{2,tip}$ versus time are also presented in a flapping cycle. As can be observed, the maximum angle of attack for the flapping frequency of 6 Hz and the constant velocity of 6 m/s is about 30°, which indicates that in some wing sections the stall have been occurred in certain time intervals, and in this angle the elastic twist has been considered.

In addition, in Fig. 13, the time history of the pitch moment M_0, which is evaluated by integrating the product of aerodynamic forces and relative position vectors with respect to center of mass, is presented. For this purpose, the position vector of each wing sections relative to the center of mass has been used. As can be seen, the overall behavior of the pitch moment is similar to that of the vertical force, and the minor differences observed in trend of these quantities are due to the difference between the positions vectors in the various positions of the wing. By comparing the time variations of the torsion angle of the wing tip $\varepsilon_{2,tip}$ with the flapping angle γ, it is found out that the phase difference between the elastic twist of the wing sections and the flapping angle is about 90°. This result can be interpreted based on the linear velocity variations resulted from the flapping motion of the wings. In fact, as an example for $\gamma = 0$ condition, the angular velocity and, consequently, the linear velocity are the maximum, and the aerodynamic forces at this moment have maximum values. Thus, the elastic torsion of the wings which are mainly influenced by the aerodynamic forces are also the maximum. The phase difference between the angle of attack α and the flapping angle γ can also be explained by the same reason (based on the maximum velocity at the angle $\gamma = 0$). However, the torsion and attack angles are in an opposite phase, because basically the wing elastic twist, in the case that the elastic axis coincides with the leading edge, has a sign opposite to the angle of attack, and it reduces and stabilizes α.

Now, the results obtained from the bond graph model of the flapping bird are presented to study its performance curves and evaluate the aerodynamic of the two-section wing in the flapping process. The evaluation criteria of aerodynamic performance that can be considered to compare the single-section and two-section wings performance including the average horizontal and vertical forces, average power consumption, and average flapping efficiency. Therefore, the effects of the torsional flexibility (GJ), flapping frequency (f_w), flapping amplitude of the wing first section (γ_1), flapping amplitude of the wing second section (γ_2), forward velocity of the bird (V_x), phase difference between the inner and outer part of the wing (Ω) and initial incidence angle of the wing (α_0) on evaluation criteria are studied. According to Table 2, in the parametric study to describe the performance of the two-section flapping wings, each of above parameters are appropriately changed around the nominal values, and for each selected value, the performance quantities, including the forces, power and efficiency are averaged in one cycle within the steady-state oscillation conditions.

Figure 14 indicates the propulsive force, vertical force and the average consumed power, as well as the propulsive efficiency of the flapping bird in terms of the torsional stiffness of the wing. As it is observed, for a certain amount of the torsional stiffness, the propulsive force and efficiency have been approximately maximized. Consequently, these desired conditions can be considered as the broader range of the angles of attack which are less than the stall angle. Regarding the effect of the torsional stiffness of the

Table 2 Parametric study quantities

Parameters	Nominal condition	Changing intervals
GJ (N cm^2)	25	5–100
f_w (Hz)	6	2–8
γ_1 (°)	30	15–60
γ_2 (°)	30	15–60
V_x (m/s)	6	2–10
Ω (°)	180	120–240
α_0 (°)	0	0–10

Fig. 14 Influence of the torsional stiffness on the average propulsive force, average vertical force, average consumed power and propulsive efficiency
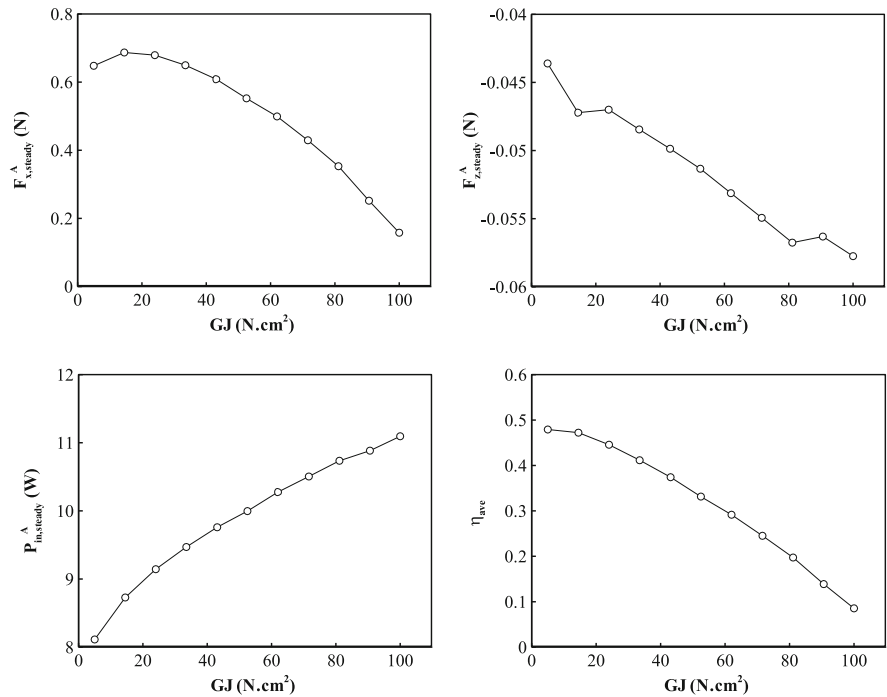
wing on the average vertical force, due to the zero initial angle of attack which was considered in the nominal condition, it is expected that the output be zero. However, the slight variations of the vertical force can be resulted from the complete asymmetry between the up and down stroke pahses. One of the major achievements is the prominent role of the torsional stiffness in changing the propulsive force that can be used as a control parameter in two-section flapping wing robots. Here, power consumption increment due to the increase in the wing torsional stiffness is correctly indicated. In fact, the reduction in torsional stiffness and the amplitude of the wing deformation leads to an increase in the range of the forces amplitudes which will facilitate the flapping process, and reduce power consumption.

The next under investigation parameter is the flapping frequency, which its effects on the aerodynamic forces, consumed power and the flapping efficiency are indicated in Fig. 15. The study of the frequency results in the interesting achievements. Up to about 3 Hz frequency, the average horizontal force is negative, which means that the propulsive force due to the wing flapping motion cannot overcome the wing and body drag forces. Therefore, at frequencies lower than 3 Hz, the aerodynamic force and, consequently,

produced power and propulsive efficiency are negative. At higher frequencies, the amount of the propulsive force is increased and the positive propulsive efficiency is achieved. Interestingly, at a frequency of about 4 Hz, the mamximum efficiency is acheived, which would be a good performance situation. The amount of the efficiency is limited to about 0.3 due to the insignificant amount of the wing flexibility, but by considering an appropriate value, this efficiency can be improved. Increasing the frequency, directly results in the double increase of the consumed power. Here, by choosing the amount of the stiffness and the flow velocity at the same values of the nominal flight, it can be seen that increasing the frequency, moderately increases the average propulsive force and then reduces it. This event is due to the occurrence of the flow separation phenomenon, which involves the wider areas of the wings over a larger time period at higher frequencies.

Figure 16 shows the variations of the aerodynamic forces, consumed power, and flapping efficiency in terms of the flapping amplitude of the first section of the wing. It is observed that choosing the amplitude in the range of about 25°–30° is desirable, despite the geometric and the performance characteristics of the flapping robot. Interestingly, similar to the frequency,

Fig. 15 Influence of the flapping frequency on the average propulsive force, average vertical force, average consumed power and propulsive efficiency
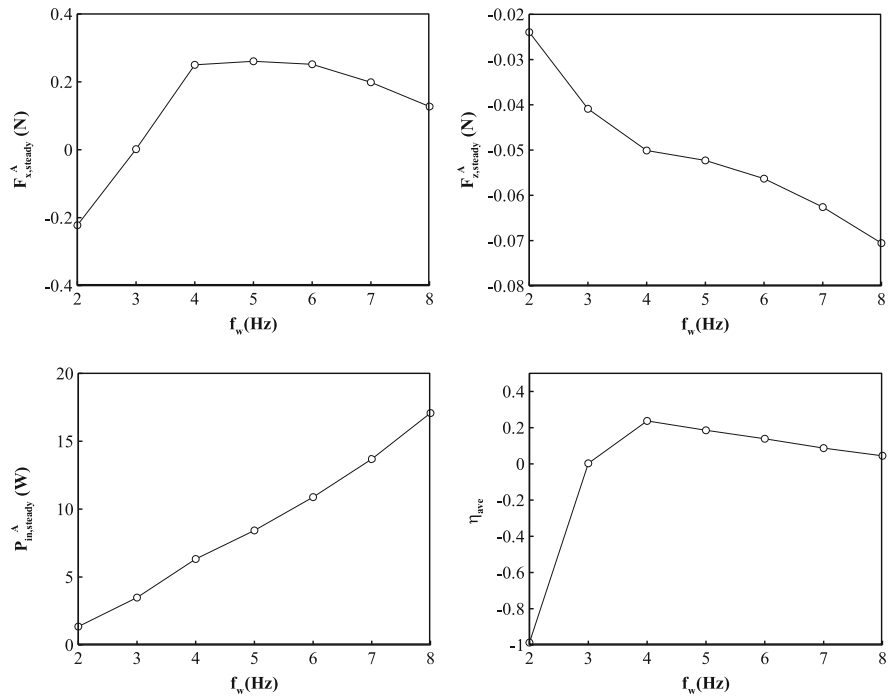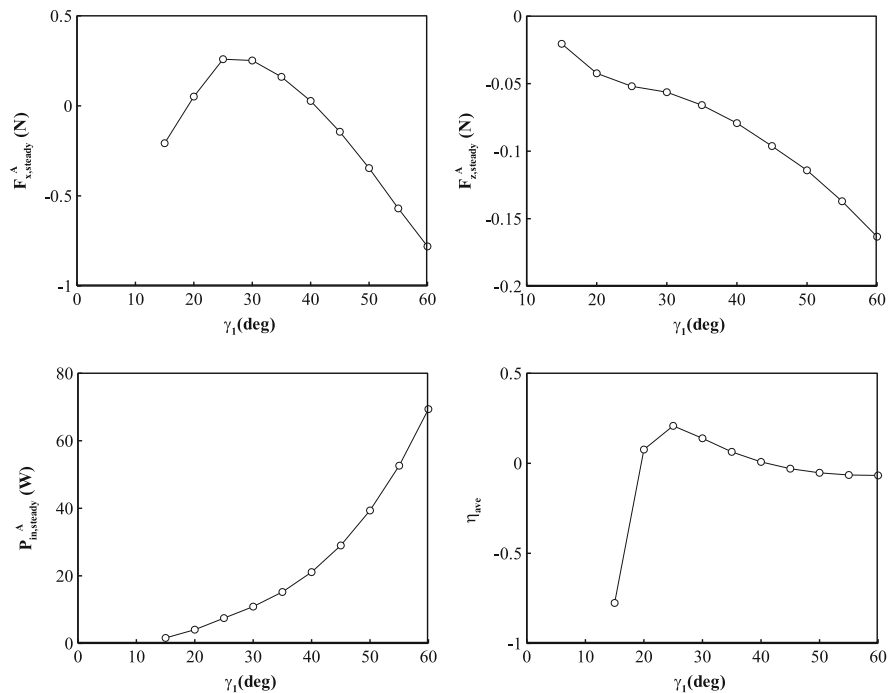

Fig. 16 Influence of the flapping angle amplitude of the wing first section on the average propulsive force, average vertical force, average consumed power and propulsive efficiency

at low flapping amplitudes, an efficient propulsive force does not essentially produce. In other words, the necessary and sufficient condition for producing the propulsive force is the presence of the considerable

amplitude and frequency simultaneously. The variations of the consumed power versus the flapping amplitude are of the second order of magnitude, because the variations of the forces amplitude with

respect to the flapping amplitude are of the second order. From the variations of the horizontal force with respect to the wing flapping amplitude, it can be understood that the desired choice of the amplitude of the wing first section is about 30° (i.e. same as the desired nominal value). Another interpretation of this desired value of the wing first section amplitude is the equality of the first and second sections amplitudes of the wings in desired out of phase conditions. Reducing the amplitude of the vertical forces by increasing the flapping amplitude and receding from the amplitude of the wing second section indicates the greater probability of the flow separation, which attenuate the aerodynamic efficiency. The greater flapping amplitude results in an increase in the angle of attack and intensifies the flow separation, which reduces both horizontal and vertical forces. In order to complete the discussion, the effects of the wing second section amplitude on the bird performance criteria are also examined.

In Fig. 17, the variations of the aerodynamic forces, consumed power and the efficiency of the flapping bird in terms of the flapping amplitude of the wing second section are presented. Regarding this figure, it can be explained that the closeness of the flapping amplitude values of the wing first and second sections

in non-phase conditions is a significant point in design. Such a similarity can be deduced from the comparison between the curves of the propulsive force and efficiency. Here, it can be observed that the behavior of the average vertical force is in contrast to the behavior of the horizontal force. It is due to the variations of the resultant flapping amplitude of the wing second section, assuming the non-phase condition of the wing both sections. Therefore, the angle of the wing second section decreases to about γ_1. In other words, sensitivity to variations of γ_1 is more than γ_2. The small amount of the average vertical force variations with respect to the flapping amplitude of the wing second section can be somehow related to the effect of the wing second section operation. Consequently, considering the larger angles helps to form the larger forces in the wing second section. Another interesting point is the effect of the wing second section amplitude on reducing the power consumption which can be interpreted due to the reduction in the total moments of inertia of the wing components around the center of rotation. Indeed, as γ_2 increases, the wing becomes closer to the folded position, and produces less moment of inertia around the flapping hinge point, which results in reducing the power consumption. However, the improved efficiency

Fig. 17 Influence of the flapping angle amplitude of the wing second section on the average propulsive force, average vertical force, average consumed power and propulsive efficiency
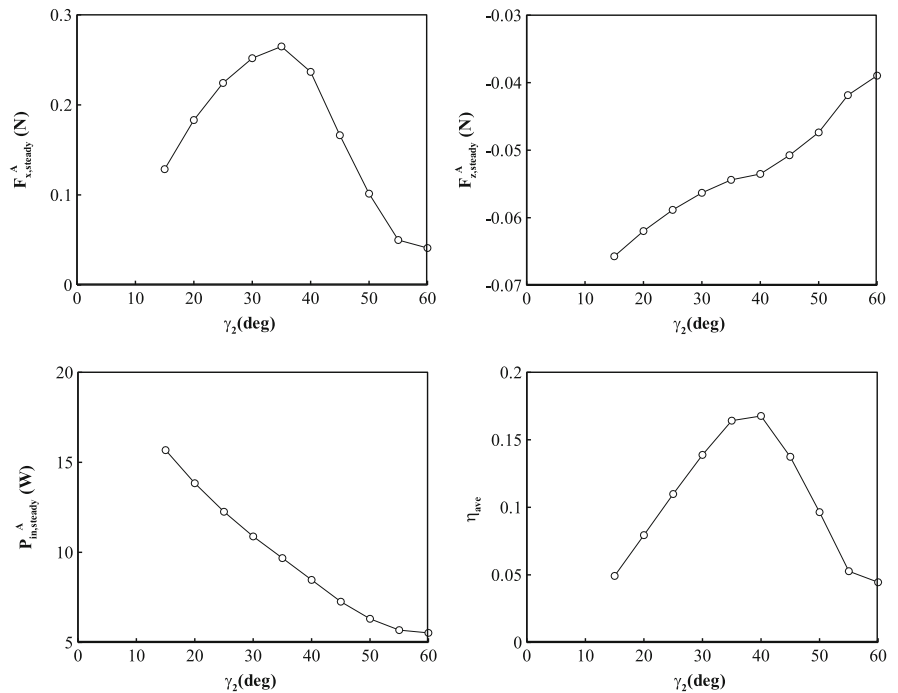
corresponds to the choice of $\gamma_2 = 40$ in the equivalent conditions to this problem.

In Fig. 18, the variations of the flapping bird performance in terms of the bird forward velocity are presented. As can be observed, increasing the velocity of the flapping wing bird improves the amplitude of the propulsive force and efficiency. Such a result is quite obvious and expected based on the analysis of a wing section with plunging motion. Nevertheless, at forward velocities higher than about 9 m/s, the amount of the drag force overcomes the propulsive force generated by the flapping motion. Hence, the trend of the resultant force will be decelerating. In fact, the cause of decreasing the vertical aerodynamic force by increasing the velocity is considering the initial angle of attack to be zero in the nominal flight conditions.

In Fig. 19, the variations in the aerodynamic forces, consumed power, and propulsive efficiency of the flapping bird are presented in terms of the phase difference between the first and second sections of the wing. An important and definite achievement is the suggestion of the wings non-phase flapping. As it can be seen, the amplitude of the propulsive and vertical forces as well as the propulsive efficiency are

improved by choosing $\gamma_2 = 180$, which corresponds to the non-phase state.

A simple explanation for these observations can be the reduction of the attack angles in the second section of the wing which is the comparative advantage of two-section wings with respect to the one-section ones. It should be noted that, in one-section wings, especially at high frequencies and amplitudes, the large portions of the wing surface are always suffering the increase in the angle of attack which results in the flow separation and stall, while in two-section wings by controlling this quantity, one can significantly improve the aerodynamic efficiency of the wing.

Figure 20 indicates the effect of the initial angle of attack on the bird performance. As expected, by increasing the wing initial incidence angle or the initial angle of the bird orientation in horizontal flight, the average amount of the produced vertical force increases which provides the bird capability to climb and carry loads. However, the average descent rate of the produced propulsive force under these conditions is small, and it can be concluded that increasing the initial attack angle which resultes from the bird trimming by the help of the tail control surface or the change in wing incidence angle causes an increase in the average lift force, and consequently in the bird

Fig. 18 Influence of the bird forward velocity on the average propulsive force, average vertical force, average consumed power and propulsive efficiency
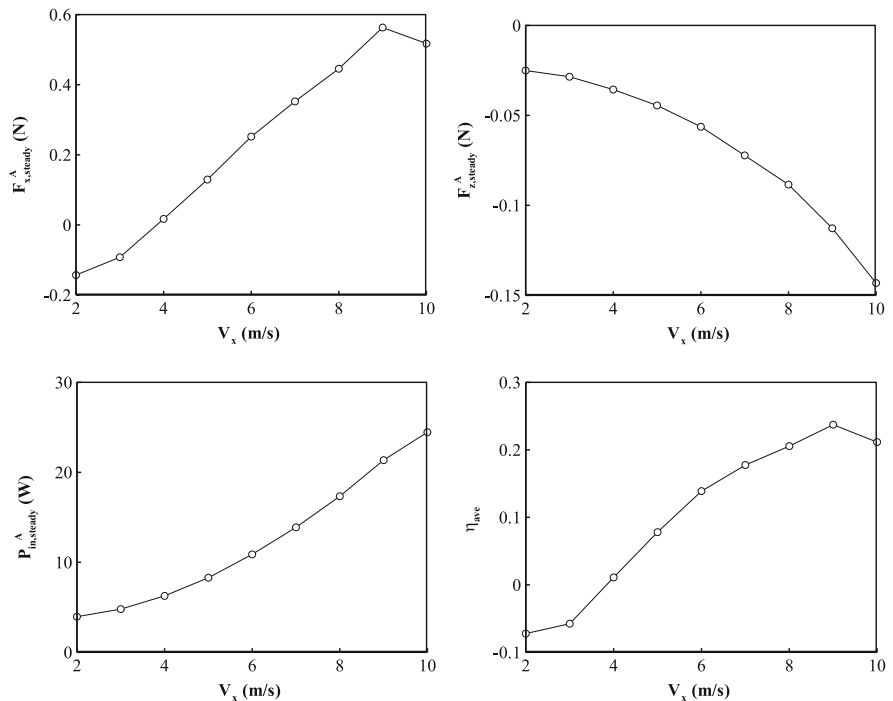
Fig. 19 Influence of the phase lag between the wing first and second sections on the average propulsive force, average vertical force, average consumed power and propulsive efficiency
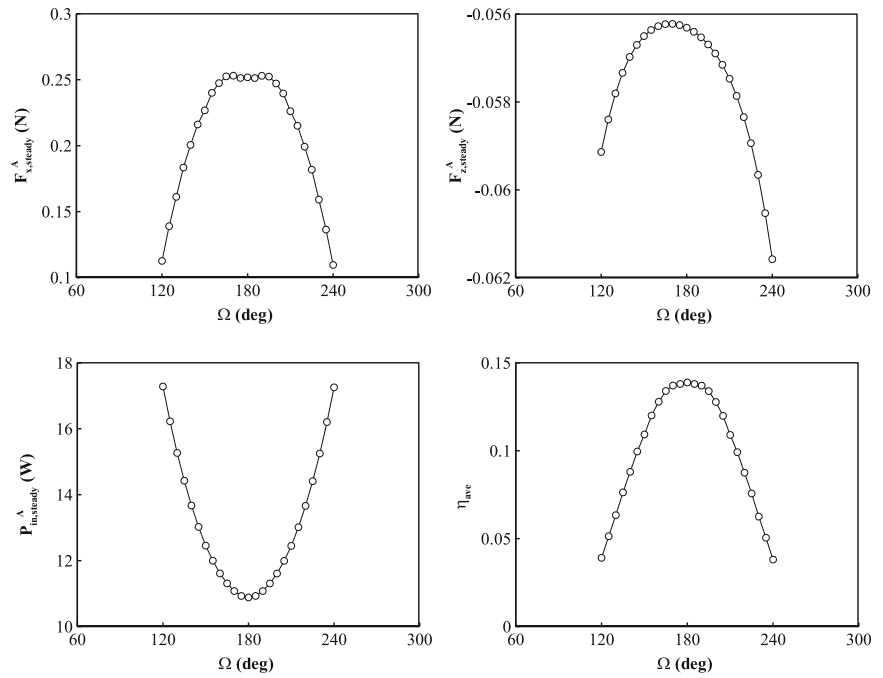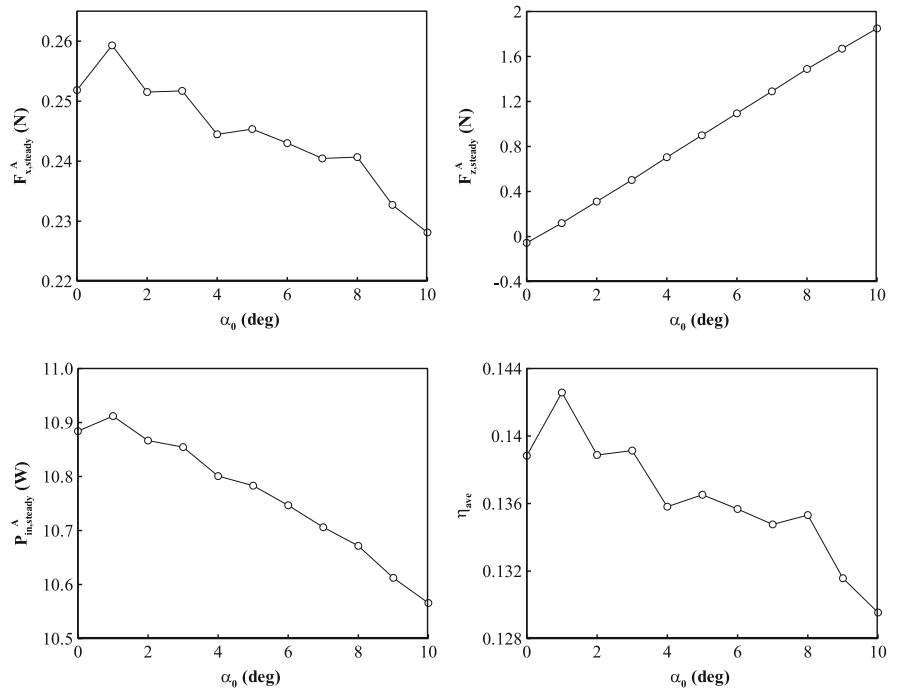

Fig. 20 Influence of the wing incidence angle on the average propulsive force, average vertical force, average consumed power and propulsive efficiency

rate of climb. Based on this curve, the wing desired incidence angle can be considered about 2° corresponding to the maximum efficiency point. The decrease in efficiency afterward is due to the further increase in the angles of attack and the flow separation

probability in areas near the wing tip or in the wider time interval of a flapping cycle. However, a slight initial angle of attack is necessary to create the positive average lift force, and therefore changing this angle can alter the relative sensitivity of the vertical and

horizontal or propulsion performance of the flapping wing bird with respect to the wing frequency. In other words, by decreasing this angle, the frequency variations mainly results in an average increase in the

propulsive force rather than increasing the average lift force.

In Fig. 21, an improved design of the flapping robot is simulated. According to the reported parameteric

Fig. 21 Variations of the propulsive force, vertical force, pitch moment, flapping angles, consumed power, useful power, wing tip angle of attack, and the wing tip twist angle versus time in desired conditions
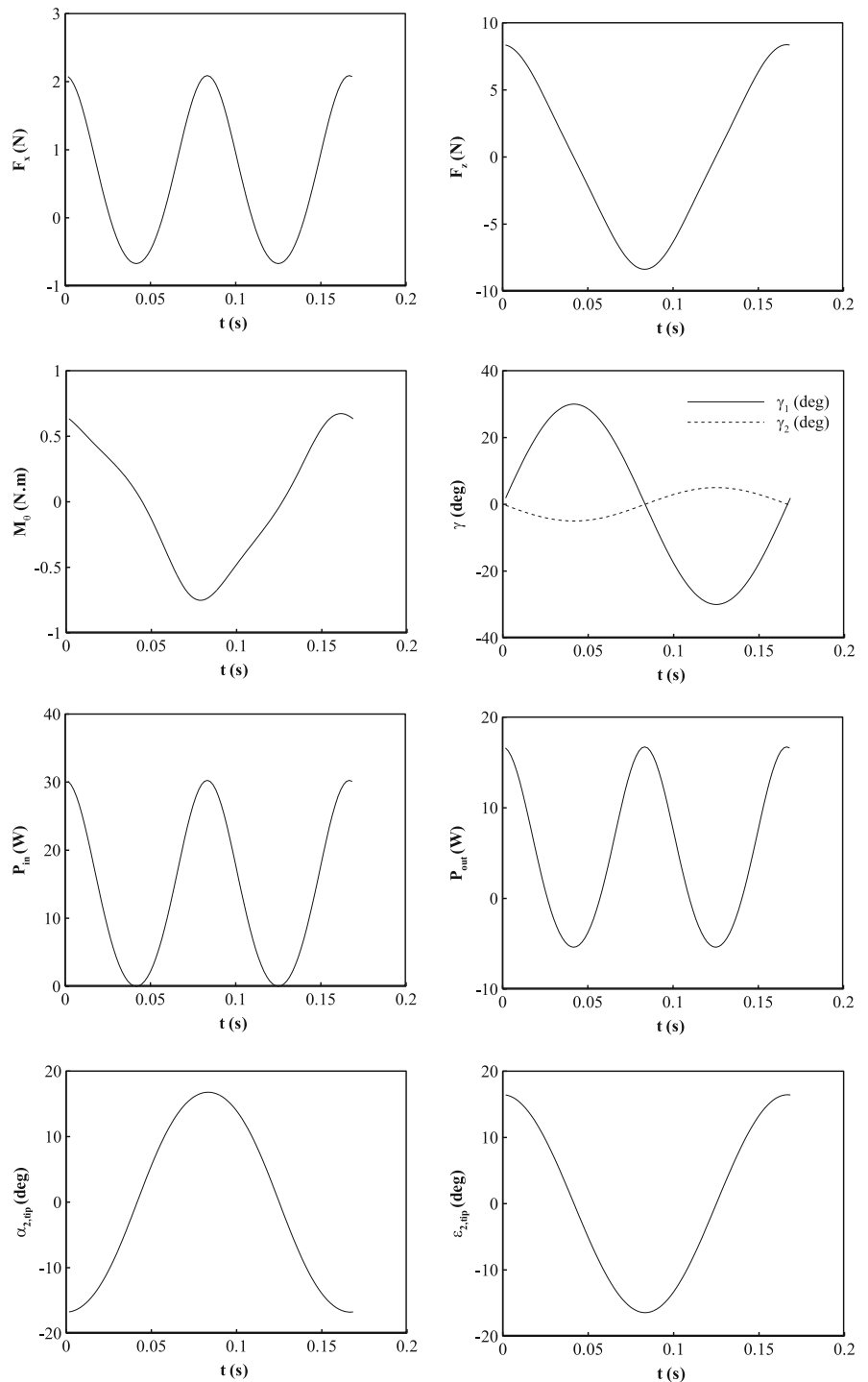
study, one may find the appropriate values of the design quantities in the vicinity of the benchmark design. The index of such tuning could be defined as the mean thrust or the propulsive efficiency. Based on these performane measurements, the new selection of the flapping amplitudes, forward velocity, phase lag of the wing second section and particularly the torsional stiffness of the wing material has been extracted. It is interesting that by a change in above design variables a considerable progress in the performance of the flying robot would be achieved without any further cost or penalty in weight. As depicted in Fig. 21 the thrust force due to flapping is enhanced comparing to the benchmark simulation in Fig. 13. Although the change in flapping amplitude and the phase-lag between the wing sections can be beneficial, the most performance sensitivity of the aeroelastic behavior of the wing structure during flapping process could be obviously remarked through the torsional stiffeness variations, and consequently the twist angle of the wing spanwise stations. Comparing the profiles of the angle of attack and twist angle in the wing tip location, in Fig. 21 and 13, reveal that adjusting angle of attack distribution by the help of tunning the two-sectin mechanism would be the key item in kinematic enhancement. Incorporating both kinematic and mechanical adjustment of the parameters mentioned in Table 3, the mean propulsive efficiency has been increased 8 percent and reached to 0.42. Computing the mean thrust force indicates more progress, which is partially due to the change in forward velocity.

4.3 Comparison between the performance of the single-section and two-section flapping wings

In this section, an important and interesting topic would be discussed which is one of the results of the present research. In this regard, the motivation for

Table 3 Efficient value of investigated parameters

| Parameters	Value
GJ (N cm^2)	5
γ_1 (°)	30
γ_2 (°)	35
V_x (m/s)	8
Ω (°)	180
α_0 (°)	0

designing and manufacturing of the articulated flapping wing can be investigated. From this point of view, we will reach to a variety of topics, including improvement and design of the wing geometries. The main question in this respect is the necessity of using an articulated flapping wing, and its efficiency and operation. To answer the question of whether the use of the articulated flapping wings can be useful and helpful or not, a qualitative and a quantitative approach can be used. From the qualitative point of view, the physics of the problem indicates that in single-section flapping wing, the probability of the flow separation is increased due to the creation of high attack angles in the wing tip areas, which increases as the wing span, flapping frequency or amplitude increase. Whereas in the articulated flapping wings by adjusting the kinematic parameters, especially the phase and amplitude differences, as well as the change in the location of the middle hinge point, such an event can be counteracted and, therefore, it results in a better efficiency. There are important points that provide the basis for an attractive design problem. On the one hand, it includes the issue of providing the sufficient lift and thrust forces and its counteraction to reduce the flow separation and stall, and on the other hand, the compromise between the added weight to the system due to the mechanism improvement and the enhancement of the aerodynamic performance, make the design of the articulated wing more complicated.

In Fig. 22, a comparison between the performances of the articulated flapping wing in various folding angles of the wing second section is presented. In fact, in this simulation, the amplitude of the wing second section is considered to be zero, which is equivalent to the assumption that the both wing sections are connected or welded together. Therefore, the only independent parameter in this case is the initial angle between the lengths of the both wing sections which the same angle would be saved. This angle can be called the wing folding angle γ_{fold}. Based on the results indicated in the above figure, it can be seen that the zero angle (equivalent to the straight and unfolded wing) is not improved for the average propulsive force. In addition, in terms of the aerodynamic efficiency, which can be considered as a more appropriate indicator, the non-zero folding angle of the wing can help to improve the aerodynamic efficiency. The improvement of the efficiency and the reduction of the power consumption by creating a

Fig. 22 Performance characteristics of the two-section flapping wing versus folding angle in the state that both wing sections are connected or welded together (passive second section)
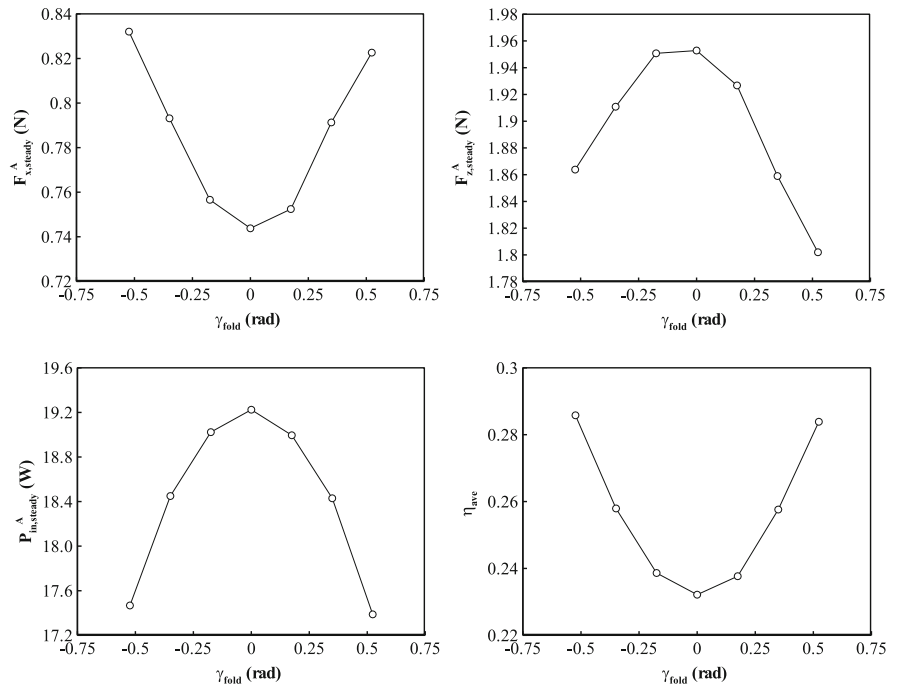
proper folding angle are about 10%. In Fig. 22, the performance variations of the articulated wing are plotted in terms of the amplitude of the wing second section. These curves are important because of their capability to provide a suitable scale between the single-section and articulated wings. In fact, the corresponding conditions to the single-section wing is the same point as $\gamma_2 = 0$, which by default in this simulation the initial folding angle is considered to be zero, and a straight single-section wing shape is produced. Increasing γ_2, which is the flapping amplitude of the wing second section, practically leads to achievement of the active articulated wing. It is observed that by activating the wing second section, the performance characteristics and especially the efficiency are improved. So, it could be understood that the usefulness and effectiveness of the articulated wings are considerable.

Figure 23 shows the performance characteristics of the flapping wing versus amplitude of the wing second section. It is observed that the appropriate value of the flapping amplitude of the wing second section is about 0.4 rad which certainly depends on the choice of $\gamma_1 = \pi/6$ in this simulation and for this particular geometry. Moreover, it is observed that the desired choice of γ_2 for specific conditions of this simulation is about 0.6 rad, and the choice of higher γ_2 values leads

to the efficiency drop. According to the adjusted value of $\gamma_1 = \pi/6$ in this simulation, it would be found out that γ_2 is equal to 0.6 rad in the sense of equalizing the flapping amplitude of the wing first and second sections. In other words, the efficiency is maximized while the second section is active with the same amplitude and in the opposite phase. In addition, it can be seen that, although considering γ_2 amplitude more than γ_1 can reduce the propulsive force and even efficiency, it can increase the average lift force. The rate of increasing the average lift force and decreasing the average propulsive force, in the range of γ_2 amplitude more than that of γ_1, are the same. However, this trend continues until γ_1 equals to about 0.8 rad. After that, the aerodynamic indices will also drop. It seems that the desired and maximum γ_2 angles can be defined at any given frequency and for any given geometry.

5 Conclusion

In this research, an integrated and systematic model of an elastic two-section flapping wing based on the bond graph approach was developed. For each of the subsystems the corresponding bond graph model was extracted, and finally by implementing the necessary

Fig. 23 Performance characteristics of the two-section flapping wing versus amplitude of the wing second section (active second section)
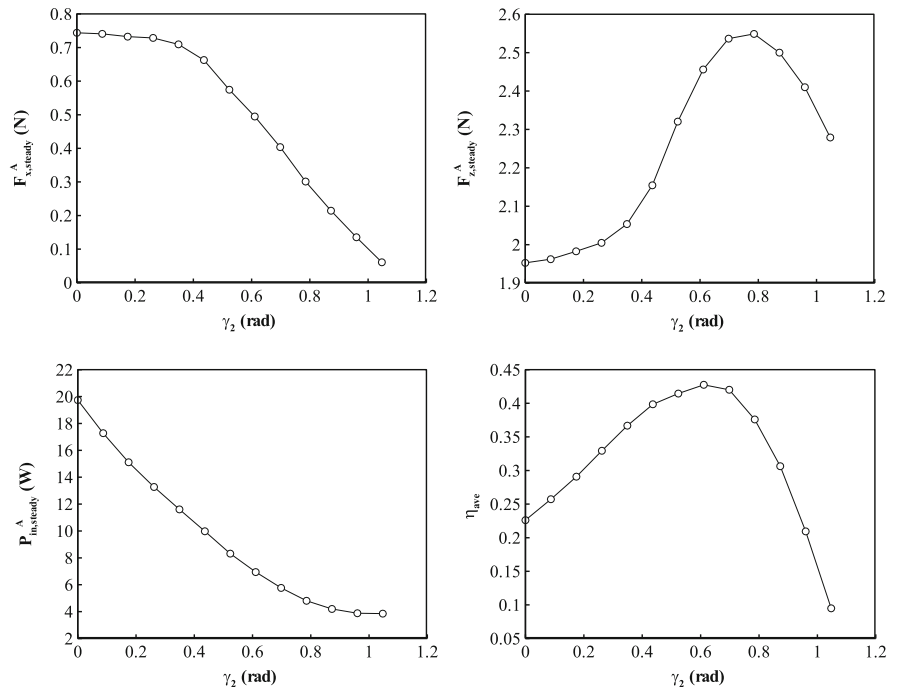
geometrical transformations and kinematic formulations of the wing motions, it becomes possible to study and to simulate the dynamics of this bird. Since there is more complexity in the flapping mechanism of the articulated flapping wings, here a simple layout with the less weight penalty was used. The aeroelastic modeling in the form of the torsional mode shapes was performed to estimate the torsional angles of the wing sections. Moreover, an appropriate describing function was utilized to calculate and correct the aerodynamic coefficients considering the stall effects. Finally, to demonstrate the capability of this bond graph model, a sample case study was performed. It was shown that for a typical flapping bird, the use of the articulated wing considerably improves the aerodynamic performance and the performance indices. The articulated wing not only can improve the bird's efficiency in energy conversion and modify the separation event in some of the wing sections at some time intervals, but it also provides a large number of control parameters that can be used to obtain the variety of flight goals such as cruise or climb. Choosing articulated wing structure, the transmission of energy to various transitional and rotational channels can be controlled restrictively. As an example, changing the flapping phase of the wing second-

section can produce more propulsive horizontal or vertical forces. Using the presented parametric study, the sensitivity of the performance parameters to the kinematic variables or mechanical properties such as stiffness were extracted and depicted. The achievement of this activity is to provide a comprehensive model that would be a suitable framework for future works in design and optimization areas.

Compliance with ethical standards

Conflict of interest The authors declare that they have no conflict of interest.

References

1. Feshalami BF, Djavareshkian MH, Zaree AH, Yousefi M, Mehraban AA (2018) The role of wing bending deflection in the aerodynamics of flapping micro aerial vehicles in hovering flight. Proc Inst Mech Eng Part G J Aerosp Eng 0(0):1–13
2. Mastro AT (2012) Design and construction of passively articulated ornithopter wings. M.Sc. Thesis, University of North Carolina at Chapel Hill
3. Kim S, Kim M, Kim S, Suk J (2018) Design, fabrication, and flight-test of articulated ornithopter. In: 10th International micro-air vehicles conference, Australia
4. Hua Z, Hou Y, Zhu J (2018) Aerodynamic analysis of three-section flapping wing by numerical simulation. In: 8th

International conference on manufacturing science and engineering, advances in engineering research, vol 164, pp 584–591

5. Ma N, He GP (2013) The simulation and aerodynamic analysis of flapping-wing MAV. Sci Technol Inform 33:1–2 **(in Chinese)**

6. Chand AN, Kawanishi M, Narikiyo T (2014) Design analysis, modelling and experimental validationof a bird-like flapping-wing flying robot. In: International micro air vehicle conference and competition, Netherlands

7. Stowers AK, Lentink D (2015) Folding in and out: passive morphing in flapping wings. Bioinspir Biomim J 10(2):025001

8. Srigrarom S, Chan W (2015) Ornithoptertype flapping wings for autonomous micro air vehicles. Aerospace 2(2):235–278

9. Shams S, Mirzavand Borojeni B, Mansoori SM, Kazemi MR (2018) Kinematic analysis of articulated flapping wings mechanisms considering nonlinear quasi-steady aerodynamic. Modares Mech Eng 17(12):87–97

10. Guerrero JE, Pacioselli C, Pralits JO, Negrello F, Silvestri P, Lucifredi A, Bottaro A (2016) Preliminary design of a small-sized flapping UAV: I. Aerodyn Perform Static Longitud Stabil Mec 51(6):1343–1367

11. Negrello F, Silvestri P, Lucifredi A, Guerrero JE, Bottaro A (2016) Preliminary design of a small-sized flapping UAV: II. Kinemat Struct Asp Mec 51(6):1369–1385

12. Send W, Fischer M, Jebens K, Mugrauer R, Nagarathinam A, Scharstein F (2012) Artificial hinged-wing bird with active torsion and partially linear kinematics. In: 28th Congress of the international council of the aeronautical sciences, Australia

13. Karnopp D (1997) Understanding multibody dynamics using bond graph representations. J Frankl Inst 334:631–642

14. Wong YK, Rad AB (1998) Bond graph simulations of electrical systems. In: International conference on energy management and power delivery, Singapore

15. Sargaa P, Hroncováa D, Curillaa M, Gmiterkoa A (2012) Simulation of electrical system using bond graphs and MATLAB/Simulink. Procedia Eng 48:656–664

16. Zhang XP, Rehtanz C, Pal B (2015) Flexible Ac transmission systems modeling and control. Springer, Berlin

17. Bontemps A, Valenciennes F, Grondel S, Dupont S, Vanneste T, Cattan E (2014) Modelling and evaluation of power transmission of flapping wing nano air vehicle. In: IEEE/ASME 10th international conference on mechatronic and embedded systems and applications, Italy

18. Poterasu V, Ibanescu R, Grigoras V (1996) Modelling of a nonlinear vibrating multibody mechanical system using

bond graph method. In: Proceedings of the 2nd European nonlinear oscillations conference, Prague

19. Bera TK, Samantaray AK (2011) Consistent bond graph modelling of planar multibody systems. World J Model Simul 7:173–188

20. Wang Z, Yang T (2014) The dynamic simulation of planar linkage with revolute joint clearance based on vector bond graph. Sens Transducers 175:321–326

21. Lee SJ, Chang PH (2012) Modelling of a hydraulic excavator based on bond graph method and its parameter estimation. J Mech Sci Technol 26:195–204

22. Bakka T, Karimi HR (2013) Bond graph modeling and simulation of wind turbine systems. J Mech Sci Technol 27:1843–1852

23. Mellal MA, Adjerid S, Benazzouz D (2011) Modelling and simulation of mechatronic system to integrated design of supervision: using a bond graph approach. Appl Mech Mater 86:467–470

24. Kazemi R, Mousavinejad I (2011) A Comprehensive model for developing of steer-by-wire system. Int J Mech Aerosp Ind Mechatron Eng 5:17–23

25. Dupont S, Grondel S, Bontemps A, Cattan E (2014) Bond graph model of a flapping wing micro-air vehicle. In: IEEE/ASME 10th international conference on mechatronic and embedded systems and applications, Italy

26. Doan LA, Delebarre C, Grondel S, Cattan E (2017) Bond Graph based design tool for a passive rotation flapping wing. In: International micro air vehicle conference and flight competition, France

27. Jahanbin Z, Ghafari AS, Ebrahimi A, Meghdari A (2016) Multi-body simulation of a flapping-wing robot using an efficient dynamical model. J Braz Soc Mech Sci Eng 38(1):133–149

28. Jahanbin Z, Karimian S (2018) Modeling and parametric study of a flexible flapping wing MAV using the bond graph approach. J Braz Soc Mech Sci Eng 40:1–19

29. Karimian S, Jahanbin Z (2019) Aerodynamic modeling of a flexible flapping-wing micro-air vehicle in the bond graph environment with the aim of assessing the lateral control power. Proc Inst Mech Eng Part G J Aerosp Eng 0(0):1–18

30. Karnopp DC, Margolis DL, Rosenberg RC (2000) System dynamics modeling and simulation of mechatronic systems. Wiley, New York

31. Pourtakdoust SH, Karimian S (2012) Evaluation of flapping wing propulsion based on a new experimentally validated aeroelastic model. Scie Iran 19:472–482